J. Fluid Mech. (1992), *vol.* 243, *pp.* 457–487
Printed in Great Britain

Numerical investigation of three-dimensionally evolving jets under helical perturbations

By J. E. MARTIN[1]† AND E. MEIBURG[2]

[1] Center for Fluid Mechanics, Division of Applied Mathematics, Brown University, Providence, RI 02912, USA

[2] Department of Aerospace Engineering, University of Southern California, Los Angeles, CA 90089, USA

(Received 19 July 1991 and in revised form 13 March 1992)

We study the three-dimensional evolution of a nominally axisymmetric jet subject to helical perturbations. Our approach is a computational one, employing an inviscid vortex filament technique to gain insight into the vorticity dynamics of jets dominated by helical vortices. For the case of a helical perturbation only, the streamwise vorticity forming in the braid is of the same sign everywhere, with the vortex helix representing streamwise vorticity of opposite sign. Owing to the helical symmetry, concentrated structures do not form in the braid. By introducing an additional periodic perturbation in the azimuthal direction, the helical symmetry is broken and we observe the emergence of concentrated streamwise braid vortices all of the same sign, in contrast to the counter-rotating braid vortices of ring-dominated jets. A Kelvin–Helmholtz-like instability of the braid vorticity layer plays a significant role in their generation. We furthermore find that the initial evolution of the braid vorticity is strongly dependent upon the ratio between the helical and azimuthal perturbation amplitudes. Smaller azimuthal perturbation amplitudes slow down the concentration process of the braid vorticity. However, we find that the long-time strength of the streamwise braid vortices should not depend on the amplitudes of the streamwise and azimuthal perturbation waves, but rather on their wavenumbers. The evolution of the helical vortex varies with the ratio between jet radius R and shear-layer momentum thickness θ. While for a jet with $R/\theta = 22.6$ and azimuthal wavenumber five, the emerging helix continuously rotates and thereby avoids instability, we observe in a jet with $R/\theta = 11.3$ the reduction of this rotation and the near exponential growth of waves on the helical vortex, characteristic of vortex helix instability.

1. Introduction

Experimental as well as theoretical work indicates the importance of both axisymmetric and helical waves in the transition process of round jets. Part 1 of the present numerical study (Martin & Meiburg 1991*a*) was hence devoted to an investigation of three-dimensionally evolving axisymmetric modes in a jet. The dynamics were assumed to be dominated by inviscid mechanisms, and consequently we employed a vortex dynamics approach that discretized the nominally axisymmetric shear layer into vortex filaments. Under a single axisymmetric

† Present address: Department of Aerospace Engineering, University of Southern California, Los Angeles, CA 90089, USA.

perturbation, we observed the roll-up of the shear layer into ring-like vortices which produced a strong strain field within the connecting layer of braid vorticity. When we imposed an additional azimuthal perturbation, both the ring and braid regions developed fully three-dimensional, unstable configurations. Counter rotating streamwise vorticity formed in the braid regions which in turn augmented the developing three-dimensionality of the ring-like vortices. The streamwise braid vorticity was observed to collapse into concentrated vortex tubes. Vortex rings, as they exist on their own, are unstable configurations (Widnall, Bliss & Tsai 1974). Depending on the ratio of jet radius to momentum thickness, we found a similar instability to occur in the ring-like vortices of the jet. The additional three-dimensionality in the vortex structure of the jet under axisymmetric perturbation led to a significant increase in the growth rate of its momentum thickness, while also having a strong effect on entrainment and mixing. As a study of axisymmetric jets cannot be complete without consideration of the helical modes, we will, in the following, focus on the evolution of jets perturbed by helical waves.

In their study of the stability of inviscid axisymmetric jets to three-dimensional disturbances, Batchelor & Gill (1962) demonstrated the importance of non-axisymmetric modes. Their analysis combined the inviscid linearized disturbance equations to give a necessary condition for the existence of unstable solutions. The condition states that for unstable solutions to exist, the function

$$Q(r) = \frac{rU'}{m^2 + \alpha^2 r^2}$$

must achieve a maximum somewhere within the fluid, where $U(r)$ is the velocity profile, and m and α are the azimuthal and streamwise wavenumber of the disturbance. While the axisymmetric disturbance satisfied the necessary condition for instability only for velocity profiles whose variation with radius r was large, non-axisymmetric disturbances satisfied the condition for instability regardless of the profile chosen. In particular, Batchelor & Gill proved for the bell-shaped velocity profile

$$U(r) = \frac{1}{(1+r^2)^2}$$

which models the downstream development of an axisymmetric jet, that only the disturbance with azimuthal wavenumber 1 is amplified. From this, it can be concluded that further downstream helical perturbations in a jet should become more amplified than axisymmetric perturbations. Michalke (1971) extended Batchelor & Gill's work by including several parameters of the flow in his analysis for profiles of hyperbolic tangent form. Although the profiles were also non-diverging, inclusion of the momentum thickness as a parameter illustrated the streamwise dependence of the jet's stability. The maximally amplified mode varied with the ratio of jet radius to momentum thickness, although for low-frequency disturbances, modes with azimuthal wavenumber of 1 were consistently more unstable than their axisymmetric counterparts. As the shear layer spreads, a continuing decrease in the ratio of jet radius to momentum thickness accompanies the downstream development of a jet. Mattingly & Chang (1974), Chan (1976), Lopez & Kurzweg (1977), Plaschko (1979), and Strange & Crighton (1983) further studied the stability characteristics of helical waves and their region of amplification for a variety of jet profiles. By writing the linearized disturbance equation in terms of the ratio of jet radius R to momentum thickness θ, Cohen & Wygnanski (1987*a*) demonstrated the significance of this ratio

for waves with azimuthal dependence. For large values of the ratio R/θ, the linear disturbance equation becomes nearly independent of the azimuthal wavenumber of disturbance. Hence, for large values of the ratio R/θ maximally amplified wavelengths and growth rates are almost identical for helical and axisymmetric disturbances. Using a quasi-parallel velocity profile, Cohen & Wygnanski demonstrated amplification of disturbances with azimuthal wavenumbers 0–6 in jets with values of R/θ as low as 13.1. However, for these values of R/θ, the axisymmetric disturbance remains the maximally amplified mode. As the ratio of jet radius to momentum thickness further decreases, the remaining amplified disturbance of azimuthal wavenumber 1 has a growth rate which diminishes, but then finally overtakes that of the axisymmetric mode for all frequencies, in agreement with the findings of Batchelor & Gill. Our earlier numerical study on axisymmetric perturbations furthermore indicates the importance of the quantity R/θ not only for the linear stability, but also for the nonlinear stability and evolution of the jet as well.

Experimental evidence for the existence of amplified helical modes appears in numerous examinations of jet flow (Moore 1977; Ko & Lam 1984; Cohen & Wygnanski 1987*a*; Koch *et al.* 1989). Several studies indicate that over a long time, helical patterns exist approximately as long as ring-like vortices (Mattingly & Chang 1974; Browand & Laufer 1975). Recent experimental investigations by Dimotakis, Miake-Lye & Papantoniou (1983) as well as Tso & Hussain (1989) show convincingly that even fully developed jets are dominated by ring-like and helical structures whose dynamics become largely independent of the Reynolds number when this parameter is large. Single helical vortices as well as helical structures of higher azimuthal wavenumber have been observed. Using large-scale vorticity peaks for the detection of organized motion, Tso & Hussain (1989) reveal the phase characteristics of axisymmetric and helical configurations and also observe a double helical pattern in the far field of a jet. Recently, Kusek, Corke & Reisenthel (1989) designed an apparatus which allows them to excite helical modes with azimuthal wavenumbers up to $+/-6$. Experiments conducted with jets seeded by $+/-1$ helical modes reveal a staggered vortical pattern. Furthermore, Corke & Kusek (1991) show the resonance of these helical mode pairs in the manner discussed by Cohen & Wygnanski (1987*b*) in their stability analysis of a jet excited by multiple azimuthal modes.

The three-dimensional wake behind axisymmetric bodies provides an interesting comparison for the vortex structure found in the axisymmetric jet. Whereas inviscid mechanisms have been demonstrated to dominate the jet's large-scale evolution, the Reynolds number does have crucial importance in determining the resulting organized motions of the wake. For Reynolds numbers lower than 400, the vortex sheet coming off a sphere has been observed to roll up into ring-like vortices (Taneda 1956; Modi & Akatsu 1984). With increasing Reynolds number, a breakdown in the individuality of vortex structures occurs while the roll-up occurs closer to the sphere. The pictures of Ilegbusi & Spalding (1984) show single helical patterns of vortex shedding in both turbulent and laminar wakes of bars and wedges at Reynolds numbers between 6.34×10^4 and 8.0×10^4. Achenbach (1974) first suggested a double helical structure when he observed the separation point rotating around a sphere's surface for Reynolds numbers above 6×10^3. However, he rejected this proposition because of its apparent violation of the circulation theorem. The flow studies by Pao & Kao (1977) on a sphere being towed in a stratified fluid at Reynolds numbers ranging from 4×10^3 to 2×10^4 demonstrate a close-ended double helical vortex configuration, where each helix has opposite azimuthal wavenumber, which satisfies such a

constraint. Monkewitz (1988) establishes the absolute instability of incompressible axisymmetric parallel wake profiles with respect to the mode $m = 1$ type disturbance. Although viscous effects appear to play a much less significant role in the axisymmetric jet evolution, a study of the helical structures within the jet could provide some insight into the evolution of the primary and secondary structures in three-dimensional wake flows as well.

The effectiveness of the inviscid vortex filament technique (Leonard 1985) for providing a clear picture of the vorticity dynamics has been established in our earlier studies of mixing layers, wakes and jets disturbed by axisymmetric modes (Ashurst & Meiburg 1988; Meiburg & Lasheras 1988, Lasheras & Meiburg 1990; Martin & Meiburg 1991*a*). We will continue to use this method to analyse the three-dimensional evolution of a nominally axisymmetric transitional jet under helical perturbations, with particular focus on the braid region between primary vortices as well as on the nonlinear evolution of the primary structures themselves. Knowledge of the large-scale vortical formations and their dynamics, in a jet subject to helical disturbance, helps to form a more thorough understanding of the jet's three-dimensional evolution, which hopefully will lead to improved strategies for the control of such flows. As a first step we will, in §2 of this paper, consider the evolution of the jet under a single helical disturbance. Subsequently, the influence of an additional azimuthal perturbation as well as the amplitudes of the two waves will be addressed. Based on the importance that the ratio of jet radius to momentum thickness had on the dynamics of the emerging structures in our earlier study, we will give particular attention to studying the influence of this parameter for the jet whose primary structure is helical in nature. Section 3 will summarize the findings. Preliminary results on the evolution of nominally axisymmetric jets perturbed by helical waves were reported by Meiburg & Martin (1991) as well as Martin & Meiburg (1991*b*).

2. Helical waves of azimuthal wavenumber 1

In following the numerical method as outlined by Martin & Meiburg (1991*a*), we represent the axisymmetric shear layer by a number of ring-shaped vortex filaments. By assigning a circulation per filament Γ_i, we attach a velocity scale to the base flow. The velocity difference between the centreline and infinity serves as our characteristic velocity. The thickness of the axisymmetric shear layer, which we take to represent the characteristic lengthscale, is determined by the core radius σ of the filaments. In terms of these units, we will analyse jets whose initial radius R is 5. Our study is based on the temporal evolution of the axisymmetric jet. We assume streamwise periodicity while advancing each of the nodes comprising the vortex filaments. For a more complete discussion on the details of the numerical method used, we refer the reader to the mixing-layer study by Ashurst & Meiburg (1988). In order to assess the accuracy of the vortex filament method employed here, we show in figure 1 the numerically calculated linear growth rates obtained for $m = 1$ disturbances and different velocity profiles characterized by various values of R/θ. These data, after conversion to spatial growth rates via a Gaster transformation, are to be compared with those provided by Cohen & Wygnanski (1987*a*). In doing so, we have to keep in mind that even for the same values of R/θ, there can be differences in the details of the velocity profiles. Comparison with Cohen & Wygnanski's figure 5 shows that the maximum growth rate obtained by the vortex filament method is too large by about a factor of three to four. This well-known phenomenon (e.g. Meiburg 1989) is

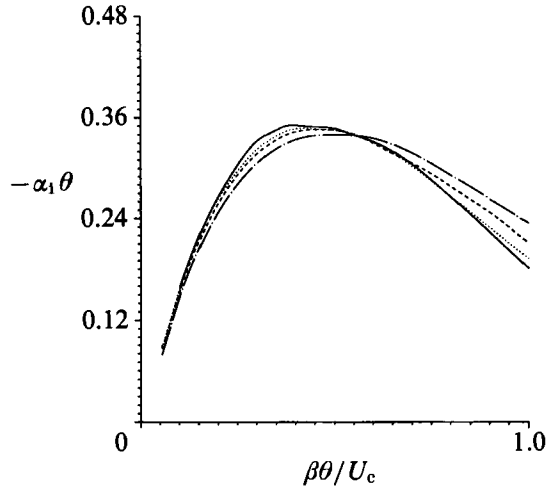

FIGURE 1. Linear growth rates obtained with the vortex filament technique for helical disturbances with $m = 1$ and a variety of velocity profiles characterized by different values of R/θ: —·—·—, $R/\theta = 6.6$; – – –, 13.1; ·····, 22.6; ——, 47.0.

primarily because the vortex filament cores do not deform under the influence of the external strain field; rather, their cross-section remains circular. However, there is a clearly defined wavelength for which the growth rate achieves a maximum value. In addition, the maximum growth rate declines with increasing smoothness of the velocity profile. Furthermore, smoother velocity profiles allow shorter wavelengths to be amplified. All of the above trends are in agreement with the results of Cohen & Wygnanski. Consequently, we can conclude that the vortex filament technique is able to duplicate the physically relevant dynamics, while it may underpredict the length of time it takes for certain events to occur. Furthermore, Martin & Meiburg (1991*a*, figures 12 and 13) present data concerning the convergence of the numerical results with improving spatial and temporal discretization which establish that the results to be discussed in the following are converged.

A jet with an initial ratio of jet radius R to momentum thickness θ of 22.6 will initiate the present analysis. This ratio determines the initial linear evolution of the jet and provides a means for comparison with the jets under axisymmetric perturbation considered earlier. Based on this value, we determine a maximally amplified streamwise wavenumber α from the calculations of Michalke & Hermann (1981), who give spatial growth rates versus non-dimensional frequency for a given value of the R/θ in inviscid jets under helical disturbance. As pointed out above, Cohen & Wygnanski provide similar data, including modes $m \geqslant 2$.

By using Gaster's (1962) transformation, we then obtain the streamwise wavelength of our control for the temporally evolving problem. For jets of $R/\theta = 22.6$ under azimuthal wavenumber-1 disturbance, the resulting wavenumber α is calculated as approximately 1. The streamwise length of our control volume is then 2π. We impose helical perturbations of azimuthal wavenumber m of the form

$$x' = \epsilon_1 R \cos(\alpha x + m\phi).$$

This perturbation displaces the centreline of a vortex filament a distance x' into the streamwise direction. ϵ_1 indicates the amplitude of the perturbation. We typically assume this amplitude to be 5% of the jet radius. Here, as opposed to the case of a streamwise displacement due to an axisymmetric perturbation considered in our

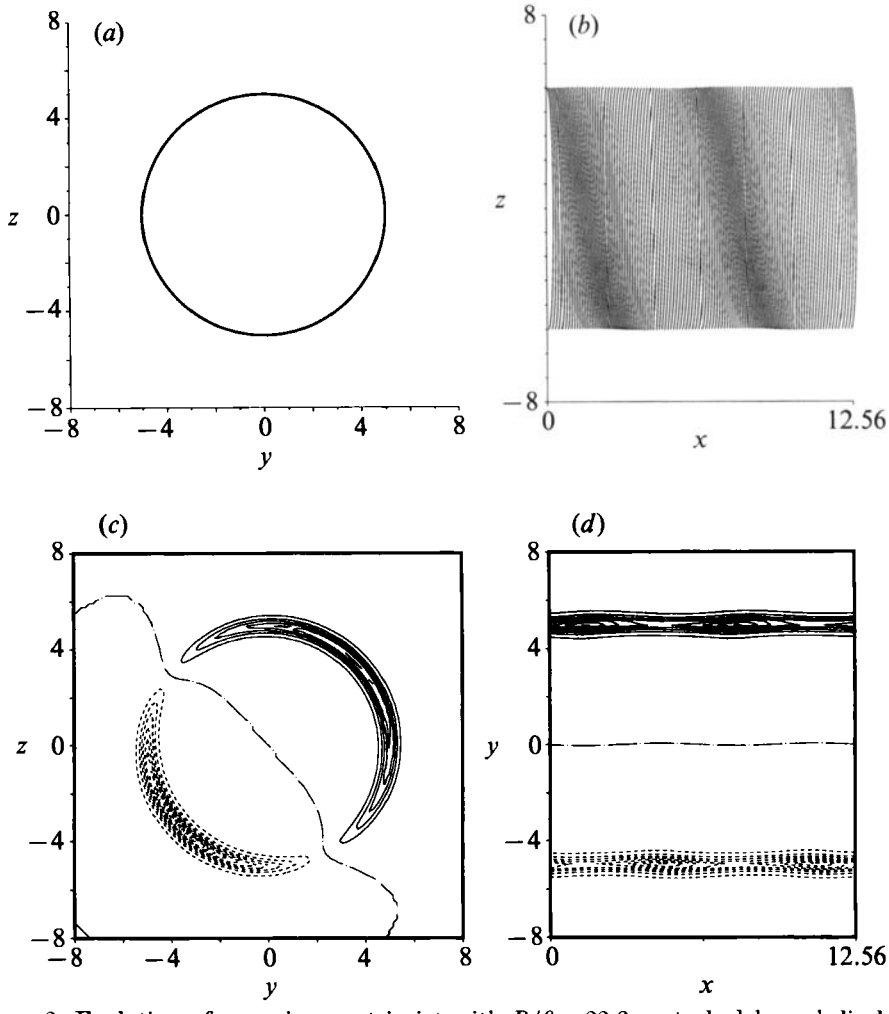

FIGURE 2. Evolution of an axisymmetric jet with $R/\theta = 22.6$ perturbed by a helical wave of azimuthal wavenumber $m = 1$: (*a*) axial view and (*b*) side view of the vortex filaments at time 0.31. For clarity, the side view displays only those vortex filament sections located at $y > 0$, but over two streamwise wavelengths. The side view indicates the nature of the helical wave. Owing to the helical symmetry of the perturbation, streamwise vorticity contours for different streamwise locations from that shown in (*c*) for $x = 4$ result under azimuthal phase shift. Circumferential vorticity contours in the plane $z = 0$ are shown in (*d*). Circumferential vorticity contours for alternate azimuthal planes result under axial phase shift.

earlier study, the displacement of a filament centreline depends on both the azimuthal and the streamwise location. The overall form of the displacement is the same for all vortex filaments. However, there is an azimuthal phase shift in successive vortex filaments which results in the helical nature of the overall perturbation.

2.1. *Helical perturbation only*

We first consider the evolution of the axisymmetric jet under a single helical disturbance of azimuthal wavenumber +1. Figure 2(*a*, *b*) displays a streamwise and side view of the filament centrelines early in the calculation at time $t = 0.31$. For clarity, we plot in the side view only those portions of the filament centrelines whose

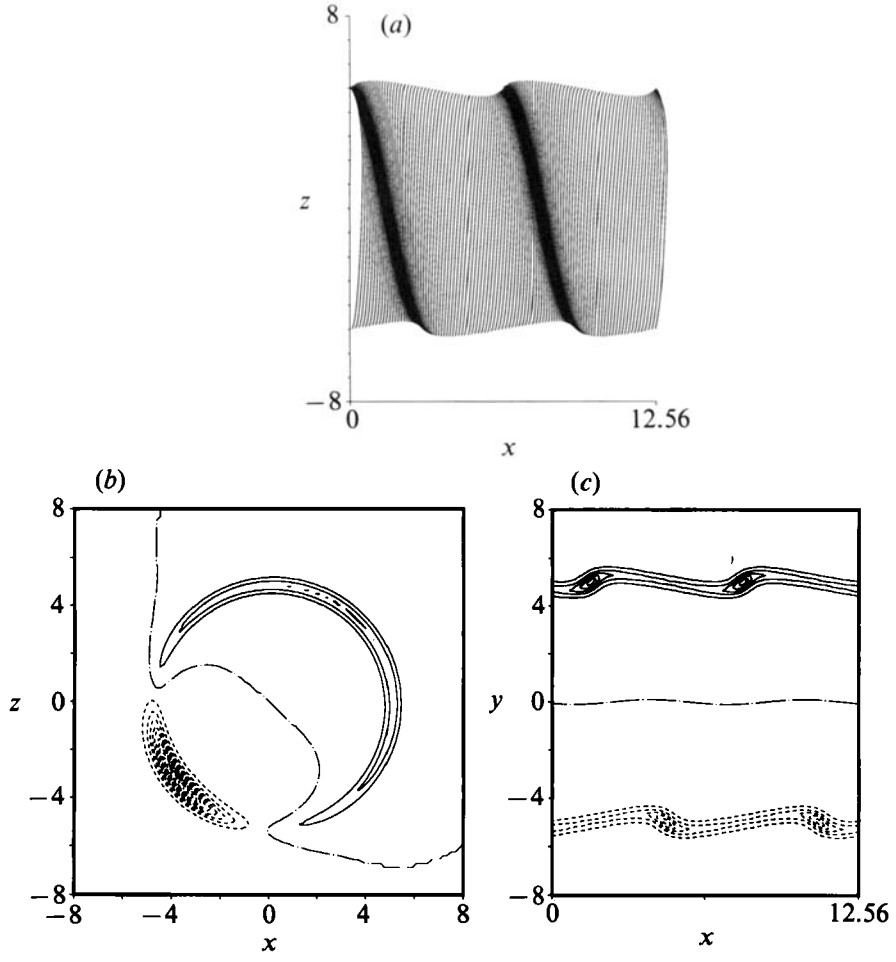

FIGURE 3. The $m = 1$ helically perturbed jet at time 2.81. (*a*) Side view of the vortex filaments. Observe the growth of a strong vortex helix, corresponding in this case to regions of negative streamwise vorticity in the streamwise vorticity contours shown in (*b*) for $x = 4$. The strain field set up by the helix leads to a reorientation of the braid vorticity, which aligns itself with the direction of extensional strain, thus resulting in positive streamwise braid vorticity. The contours of the circumferential vorticity shown in (*c*) display the cores of the emerging vortex helix.

location in y is greater than zero. Two streamwise wavelengths are shown. The helical nature of the initial streamwise perturbation can already be seen from the side view of the filaments. A contour plot of the streamwise vorticity at streamwise location $x = 4$ for this time is shown in figure 2(*c*). The streamwise vorticity is indicative of the initial perturbation. The helical symmetry of the initial perturbation persists in the evolution of the flow. By calculating the streamwise vorticity at one axial location, the view at all other axial locations results from a simple azimuthal phase shift. The same type of symmetry exists for planes of constant azimuth. Figure 2(*d*) shows the circumferential vorticity in the plane $z = 0$. Different azimuthal planes exhibit the same distribution with an axial phase shift. Helical symmetry mandates that one azimuthal or axial plane be characteristic of all other planes.

At time $t = 2.81$, figure 3 displays the roll-up of the vorticity layer into a strong helical vortex. The nominally axisymmetric shear layer undergoes a Kelvin–Helmholtz-like instability, with vorticity concentrating into a helix. As in the case

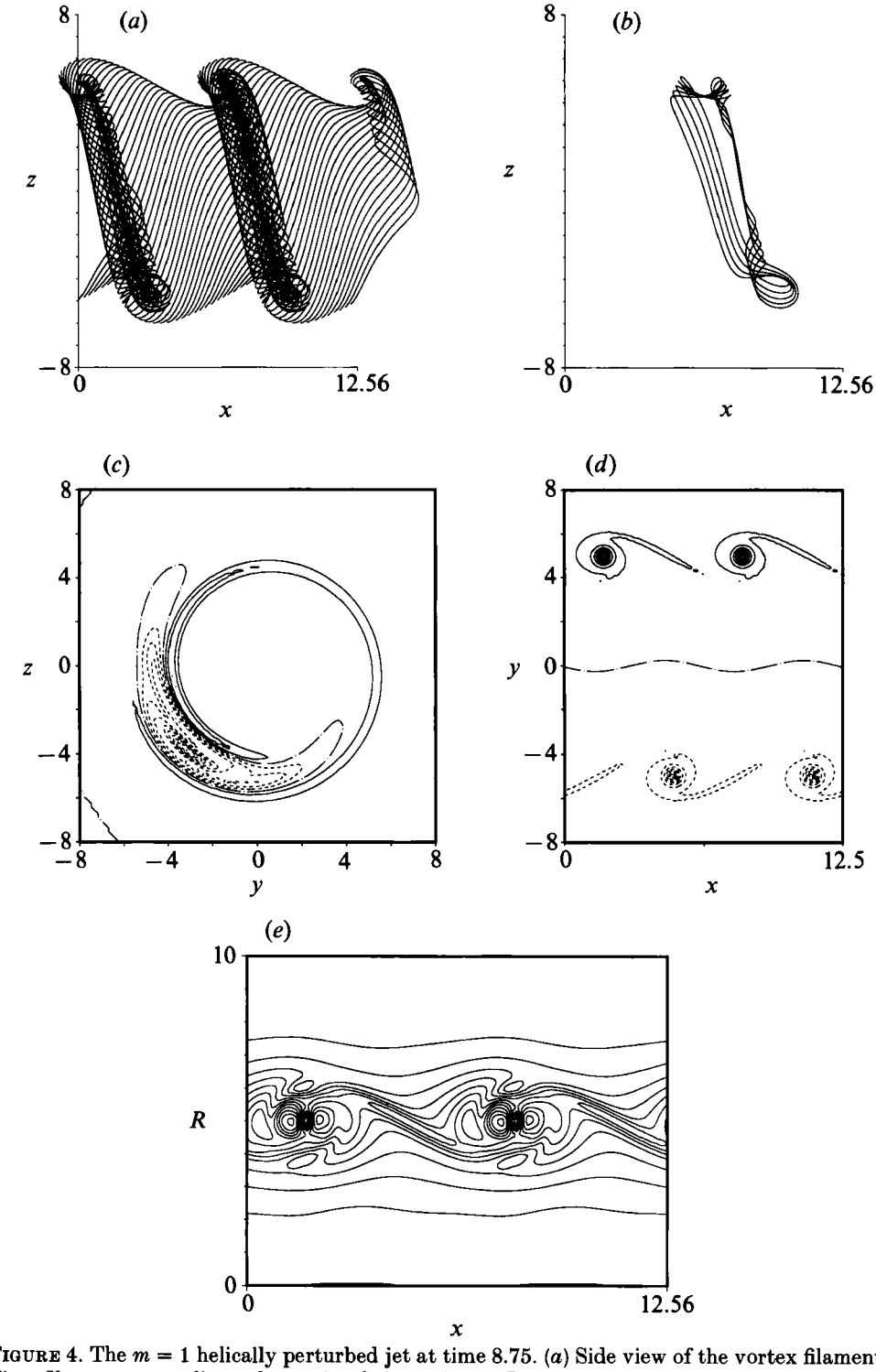

FIGURE 4. The $m = 1$ helically perturbed jet at time 8.75. (*a*) Side view of the vortex filaments. (*b*) Five filament centrelines shown in their entirety. In contrast to ring-dominated jets under azimuthal perturbation, no concentrated streamwise structures emerge. Owing to the helical symmetry of the problem the braid vorticity appears as a sheet-like layer of positive vorticity in the streamwise vorticity contours in (*c*) at $x = 4$, while the helix slices through the plane and creates

of axisymmetric perturbation, a strain field with a free stagnation point forms in the braid region between successive segments of the helix. However, the stagnation line itself is now a helix. The axis of extensional strain correspondingly orients itself in the braid region, approximately normal to the emerging helical vortex. The vorticity layer wraps around the helical structure, reinforcing it, as the resulting strain field begins to deplete the braid region of its vorticity. As the braid vorticity reorients itself in the strain field of the growing helix, streamwise vorticity becomes increasingly generated. Figure 3(*b*) shows the corresponding alteration in the streamwise vorticity. The concentrated region of negative streamwise vorticity represents the helix intersecting the plane, whereas the weaker layer of positive streamwise vorticity indicates the presence of the braid vorticity. The circumferential vorticity contours shown in figure 3 illustrate the evolving cross-sectional dimensions of the helical vortex. The two regions of opposite-signed streamwise vorticity are reflected in the configuration of a single vortex filament. Each filament, as it must remain closed under inviscid dynamics, is part of the helix in one region and part of the braid in some other region. Where it is a part of the helix, the streamwise vorticity component of the filament is of opposite sign to where it represents a part of the braid.

The evolution has become more pronounced at time $t = 8.75$. The side view in figure 4 displays the continued progression of vorticity into the helical vortex. Five vortex filaments are also shown in their entirety. Because of the helical symmetry of the present problem, no concentrated streamwise vortices can form in the braid region. Whereas in ring-dominated jets, an azimuthal perturbation leads to both signs of streamwise vorticity in the braids, the streamwise braid vorticity in helically perturbed jets is of a single sign, which is opposite to that of the streamwise vorticity of the helix. The streamwise vorticity contours of figure 4 indicate the sheet-like nature of the braid vorticity. The braid vorticity layer itself has the form of a flattened sheet of helical nature, occupying the space between the vortex helix. In contrast to the jet dominated by ring-like vortices, the principal axis of extensional strain in the braid region now has an additional circumferential component. As the braid vorticity increasingly orients itself along the direction of extensional strain, more positive streamwise braid vorticity is generated. The braid vorticity appears to spiral around the concentrated negative region of streamwise vorticity, as the layer of braid vorticity begins to wrap around the helical vortex.

Meanwhile the circumferential vorticity contours illustrate the ongoing depletion of braid vorticity by the vortex helix. The upstream neighbourhood of the vortex helix experiences a stronger depletion of vorticity than the corresponding downstream neighbourhood. In our earlier study, we discussed this effect of the jet curvature on the strain field of the ring-dominated jet. The curvature shifts the free stagnation point towards the jet axis, and thus results in greater extensional strain in the braid region upstream of a ring-like vortex than downstream. In figure 4(*e*), we provide contours of the eigenvalue of maximum extensional straining in the plane $\phi = 0$ at time 8.75. The upstream neighbourhood of the helical vortex undergoes slightly more intensive extensional strain than equivalent downstream locations. Again, the stagnation point is shifted within the connecting braid region as compared

a concentrated region of opposite-signed streamwise vorticity. (*d*) Contours of the circumferential vorticity. They show the formation of a vortex helix with round cores as well as the more intense depletion of the upstream neighbourhood of the helix. (*e*) Contour plot of the size of the positive eigenvalue of the deformation tensor at time 8.75. Greater extensional strain occurs in the upstream neighbourhood of a helix leading to greater depletion of vorticity in that region.

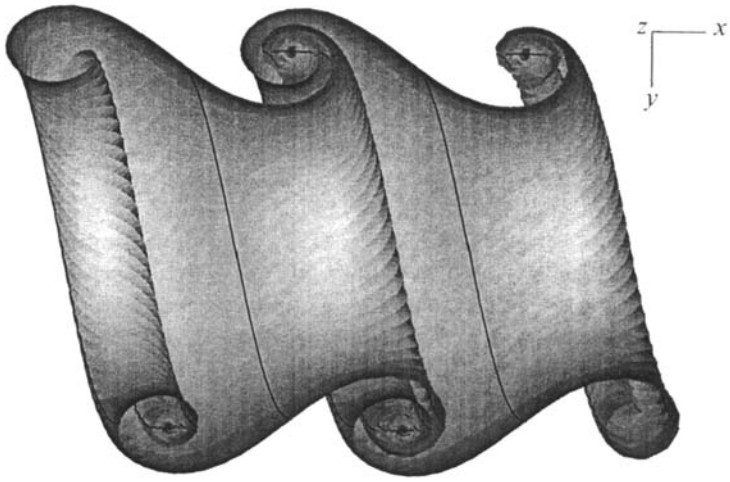

FIGURE 5. Nodes of the filament centreline with $z > 0$ are connected to form a surface. Furthermore, the stagnation line is shown in the frame of reference moving with the phase velocity of the vortex helix.

to plane mixing layer, creating a streamwise asymmetry in the overall extensional strain field of the jet. Figure 4(*e*) is consistent with the braid's depletion of vorticity. Greater depletion of the braid vorticity can then be expected upstream of the vortex helix. Tso & Hussain (1989), in their study of organized structures in a fully developed jet, reported on a similar finding. Their measurements of ensemble-averaged shear strain rate

$$\frac{1}{2}\left(\frac{\partial\langle v\rangle}{\partial x}+\frac{\partial\langle u\rangle}{\partial r}\right)$$

displayed marked variation upstream and downstream of the helical structure. Where the shear strain rate was strong, intense small-scale turbulence production and mixing occurred. In figure 5, the nodes of the filament centrelines, whose z value is greater than zero, are connected to form a shaded surface. We furthermore plot the stagnation line in the frame of reference moving with the velocity of the evolving helical structure. The stagnation line appears in the braid, parallel to the successive regions of the helical vortex. The helical nature of the stagnation line is apparent. At this time, the braid vorticity has wrapped around the helix several times, thus leading to significant stretching of the vortex filaments.

In terms of the analysis by Lin & Corcos (1984), the braid vorticity layer has an infinite aspect ratio, as peeling the braid vorticity layer away from the vortex helix would reveal an infinite sheet. Lin & Corcos, as well as Neu (1984), discuss the evolution of the braid region for the case of the plane mixing layer. Their study selectively isolates the braid regions as a two-dimensional layer of vorticity undergoing a constant plane strain. They find that the resulting evolution of a vortical braid region strongly depends on its aspect ratio, which is defined as the spanwise extent of a region of streamwise vorticity of one sign divided by its thickness. Increasingly larger aspect ratio sheets, under the action of strain and viscosity, collapse into concentrated vortices for increasingly smaller non-dimensional circulation strength. In our earlier study, we demonstrated the applicability of their results to the jet. The finite aspect ratio of the braid vorticity in the ring-dominated jet allowed for the emergence and subsequent collapse of counter-rotating braid structures. The helix-dominated jet, on the other hand, provides an analogous

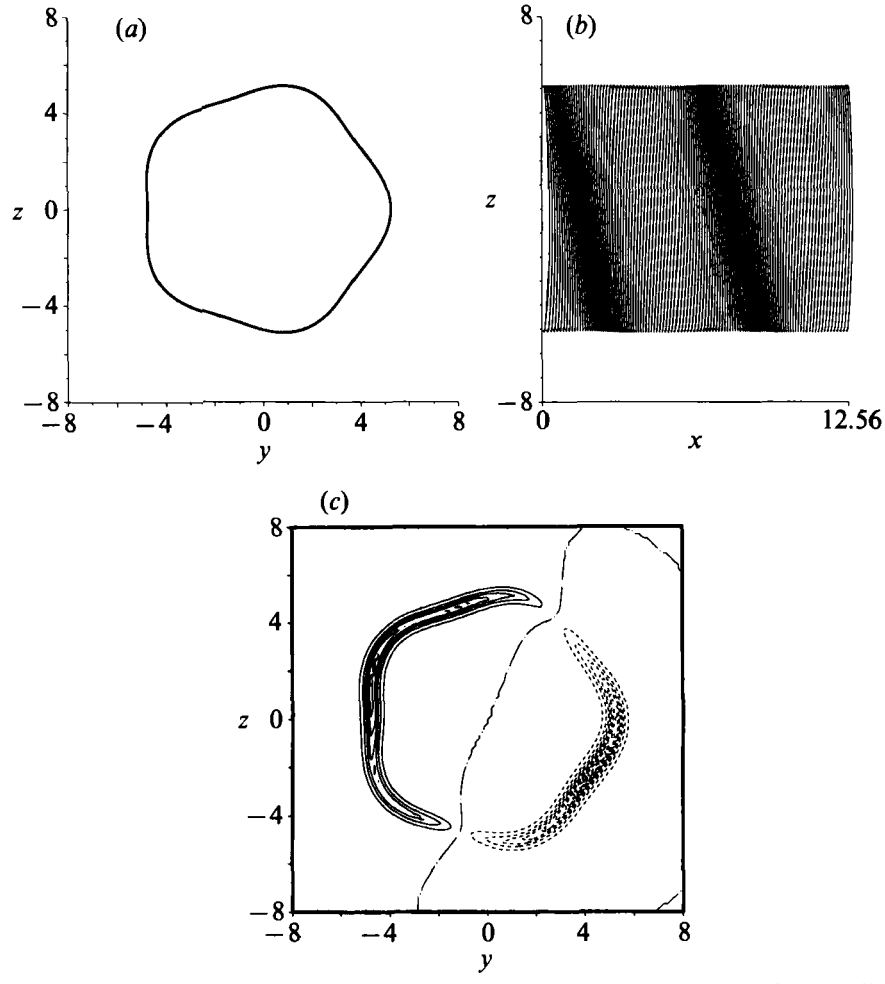

FIGURE 6. Evolution of an axisymmetric jet with $R/\theta = 22.6$ perturbed by a helical wave of azimuthal wavenumber $m = 1$ as well as by an additional azimuthal wave that introduces radial perturbation vorticity corresponding to a corrugated nozzle: (*a*) axial view and (*b*) side view of the vortex filaments at time 0.31. The axial view indicates the form of the azimuthal wave. The azimuthal wave breaks the helical symmetry. The contours of streamwise vorticity shown in (*c*) display the resulting modulation of both the positive layer of sheet-like braid vorticity and the opposite-signed region of the helix at $x = 2$.

situation to the infinite-aspect-ratio braid vorticity layers of the Lin & Corcos study. They predict that, rather than forming counter-rotating streamwise braid vortices, a perturbed infinite strained vortex sheet will redistribute into vortices of a single sign of circulation. This suggests that instability within the braid region of a helix-dominated jet will evolve differently from that which occurs in ring-dominated jets. In the following section, we will analyse the fully three-dimensional evolution by breaking the helical symmetry of our flow.

2.2 *The effect of nozzle corrugation*

In the case previously considered (Martin & Meiburg 1991*a*) of a jet dominated by vortex rings, we introduced an additional periodic radial displacement, thus simulating the jet emerging from a corrugated nozzle. We observed instabilities of

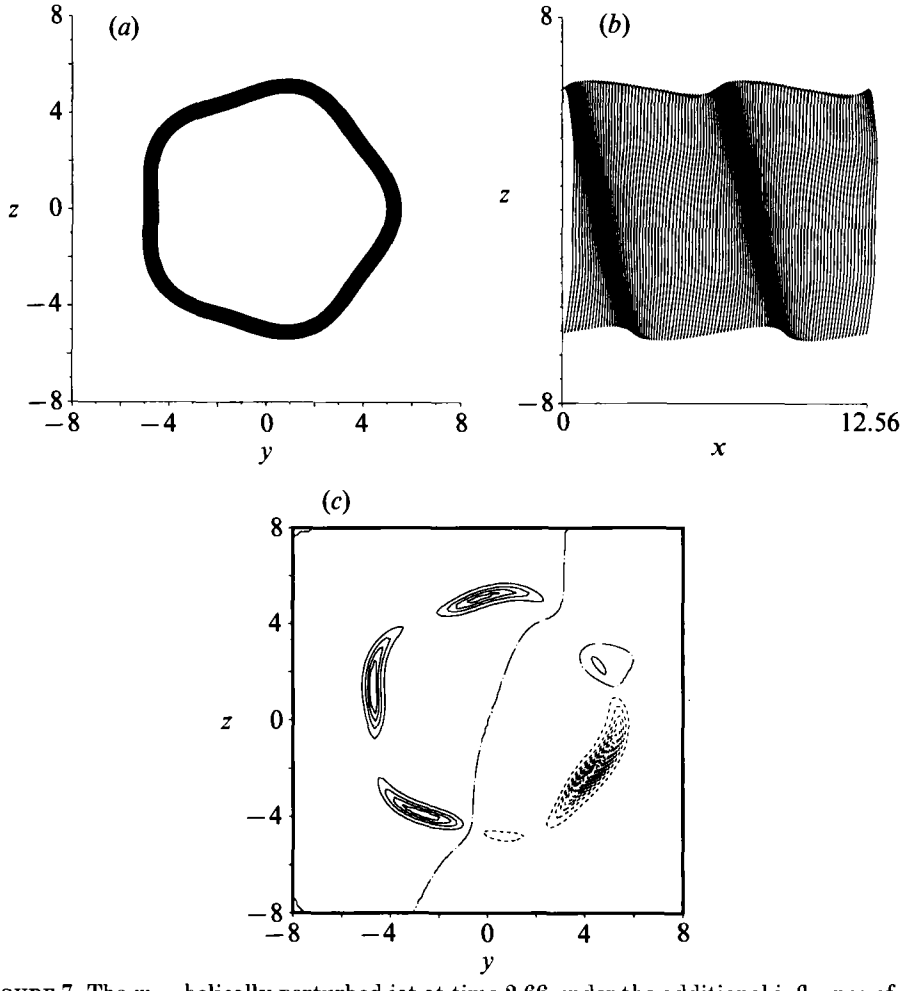

FIGURE 7. The m = helically perturbed jet at time 2.66 under the additional influence of a periodic perturbation in the azimuthal direction: (*a*) streamwise view and (*b*) side view of the vortex filaments. As a result of the additional azimuthal wave, the sheet-like braid vorticity undergoes a Kelvin–Helmholtz instability and concentrated streamwise vortices form in the braid region of the streamwise vorticity contour shown in (*c*) at $x = 2$. In contrast to jets dominated by vortex rings, the streamwise braid vortices are all of a single sign.

the ring-like vortices and the secondary braid structure of the jet. The different form of these structures under helical perturbation raises the question of their stability under an identical, added azimuthal perturbation. Several possibilities exist for instability in helical vortices. Widnall (1972) has demonstrated both long- and short-wavelength instabilities occurring in helical filaments, plus an instability that exists due to the induction of successive segments of the helix. Furthermore, the discussion by Pierrehumbert & Widnall (1982) of a translative instability of multiple spanwise rollers suggests the possibility of a helix instability as well, as the strain field existing between successive segments of the helix is similar to that generated by spanwise roller in a plane mixing layer.

We again choose as our base flow a jet with ratio $R/\theta = 22.6$ and perturb it with the helical wave of §2.1. We include an additional azimuthal perturbation of radial component only, thereby breaking the helical symmetry of the problem while

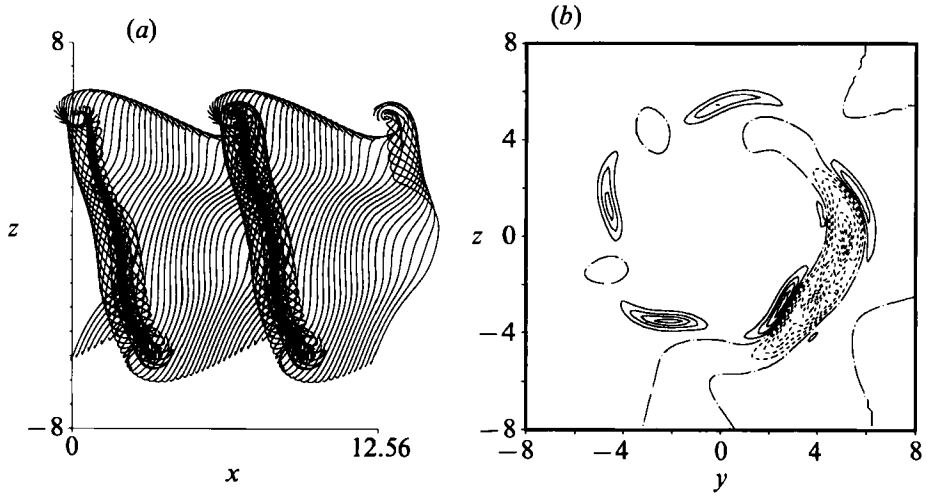

FIGURE 8. The $m = 1$ helically perturbed jet at time 7.89 under the additional influence of a periodic perturbation in the azimuthal direction. While the radial corrugation of the vorticity field shows no evidence of growth, the side view of the vortex filaments in (*a*) shows a developing streamwise modulation in the vortex helix. (*b*) Contours of the streamwise vorticity at $x = 2$. Notice the increasing strength of the streamwise braid vortices under the Kelvin–Helmholtz instability occurring in the braid region.

simulating nozzle corrugation. Therefore, in addition to the streamwise dislocation of the helical wave, filament centrelines are displaced periodically in the radial direction. The radial location of a filament centreline is then given by

$$r = R(1 + \epsilon_2 \cos(n\phi)).$$

As the wavenumber n of the corrugation we select the value 5, and ϵ_2 is taken to be 0.05. The streamwise view of the vortex filaments at time $t = 0.31$ (figure 6) displays the shape of the corrugation. The side view of the filaments shows the developing concentration of vorticity into the helical pattern reminiscent of figure 2. Contours of the streamwise vorticity at $x = 2$ illustrate the symmetry breaking effect of the added azimuthal perturbation. The result is a wavy modulation of both the emerging layer of positive braid vorticity and the beginning trace of the concentrated negative region of streamwise helix vorticity. Initially, the ring-dominated jet, under identical corrugation, developed counter-rotating braid structure. In contrast, the streamwise braid vorticity of the helix-dominated jet initially has the form of one elongated, smooth layer of a single sign.

At time $t = 2.66$, the side view in figure 7 shows the roll-up of vorticity into a concentrated helical vortex. The streamwise view of the filaments demonstrates the spread of the shear layer. Little to no growth in the corrugation is evident. The streamwise vorticity contours show concentrated structures, all of a single sign, forming within the braid region. This is in marked contrast to the resulting counter-rotating streamwise vortex pairs of the ring-dominated jet. The initial formation of the braid vorticity layer into a single-signed thin vorticity layer suggests that a Kelvin–Helmholtz instability causes the braid structures to form. The same instability mechanism is then responsible for the primary and secondary structure in a helix-dominated jet. Figure 8 of Lin & Corcos' study of the mixing layer displays a two-dimensional braid vortex of large aspect ratio taken from a counter-rotating pair. The trace of a similar Kelvin–Helmholtz instability appears to occur within the

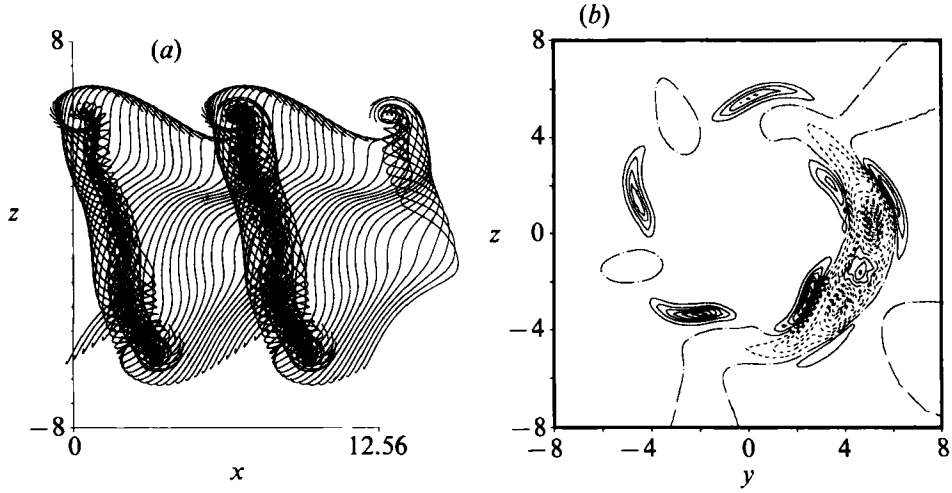

FIGURE 9. The $m = 1$ helically perturbed jet at time 10.23 under the additional influence of a periodic perturbation in the azimuthal direction. (*a*) Side view of the vortex filaments. The streamwise amplitude of the modulation along the helix continues to increase, thereby creating an alternating sign along the azimuthal extent of the vortex helix in the streamwise vorticity contour shown in (*b*) for $x = 2$.

vortex. The small scale upon which the instability develops does not allow for its adequate resolution. Lin & Corcos furthermore consider the case of an infinite-aspect-ratio sheet. The circulation of the layer of vorticity is kept uniform along the length of the sheet, thereby giving the vortices their infinite aspect ratio. By slightly perturbing the braid vorticity layer, streamwise structures result, similar to the ones we see in the helix-dominated jet. Braid vortices emerge, all of a single sign of circulation. The Lin & Corcos analysis, however, sets the strain felt by a streamwise braid vortex to a constant value. By selectively analysing the streamwise braid vortices only, their study does not account for the effect that these increasingly concentrated, single-signed vortices have on the primary structures.

Figure 8 displays the evolution of the jet at time $t = 7.89$. The streamwise vorticity contours show the single-signed braid vortices' concentration. The Kelvin–Helmholtz instability, along with the extensional strain field set up by the vortex helix, continue to strengthen the single-signed braid vortices. The side view shows the helical vortex beginning to deviate slightly from exact helical form. Owing to the added radial displacement, the evolution of the streamwise vorticity of the vortex helix is subject to the competing effects of local and global induction. As discussed in Martin & Meiburg (1991*a*), if local induction is to dominate, regions of high curvature along the vortex will acquire increased velocity. Global induction in the jet opposes local induction by decreasing velocity with decreasing proximity to the jet axis. The side view at time $t = 7.89$ shows portions of the helical vortex, located at larger radius and with greatest curvature, overtaking neighbouring portions located closer to the jet axis. This suggests that, for the present parameters, local induction plays a major role in determining the helix's early evolution.

The streamwise modulation of the helix suggests the possibility of further instability leading to the growth of these small perturbations due to the overall strain field. Based on the analyses by Widnall (1972), Widnall *et al.* (1974) and Pierrehumbert & Widnall (1982), we can only suggest how their results might apply to the jet with a single vortex of helical form. Again it is pointed out that the strain

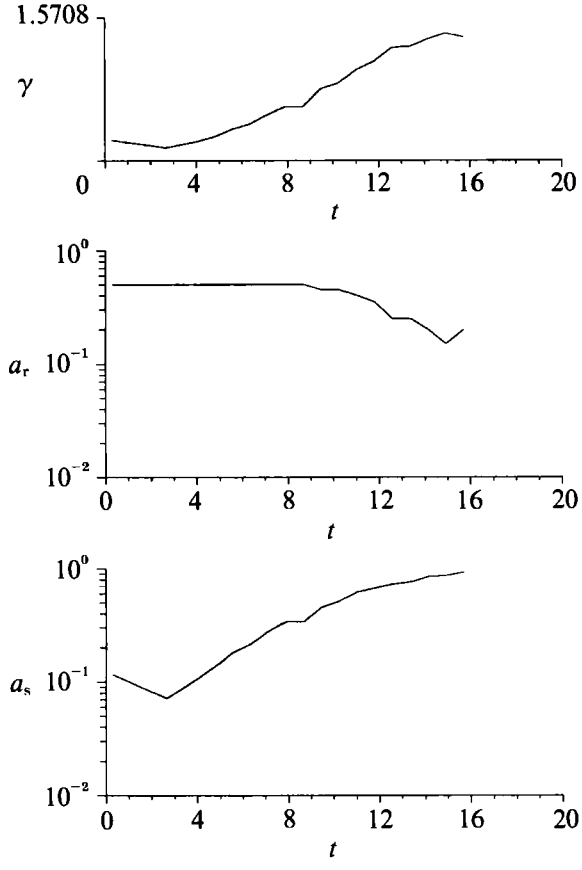

FIGURE 10. The temporal evolution of the radial amplitude a_r of the vortex helix waviness and the streamwise amplitude a_s of the vortex helix's deviation from a perfect helix of equal streamwise wavelength. Also plotted is the value γ, where $\tan(\gamma) = a_s/a_r$. The evolving vortex helix rotates continuously, thereby preventing instability.

field that exists between successive helix segments has an additional azimuthal component. If an instability similar to the one observed in the ring is to occur in the helix, we expect the helix's deviation from its unperturbed form to grow in an exponential fashion. In particular, we expect such an instability to occur as the rotation rate of the helix in the overall strain field vanishes, since such an elimination of rotation was deemed necessary for the Widnall-type vortex ring instability as well. Under these circumstances, wavy perturbations can grow in the stagnation point flow created by the rest of the helix, so that helical vortex instability can result.

Figure 9 shows the resulting flow at time $t = 10.23$. The region of concentrated streamwise vorticity of the helix now begins to alternate in sign in the streamwise vorticity contour plot, thus indicating that the helix now changes streamwise direction along its extent. From the side view, it is apparent that the streamwise modulation in the helical vortex continues to grow. To investigate the stability of the helix, we consider the evolution of the amplitudes of the streamwise and radial deviations of the vortex helix centreline from exact helical shape. We compute the circumferential vorticity of the vortex helix at successive ϕ = constant planes in increments of 4.5°. The centreline of the vortex then connects the successive locations of maximum circumferential vorticity. In figure 10 we plot, as a function of time, the maximum displacement between the streamwise location of the helical vortex's

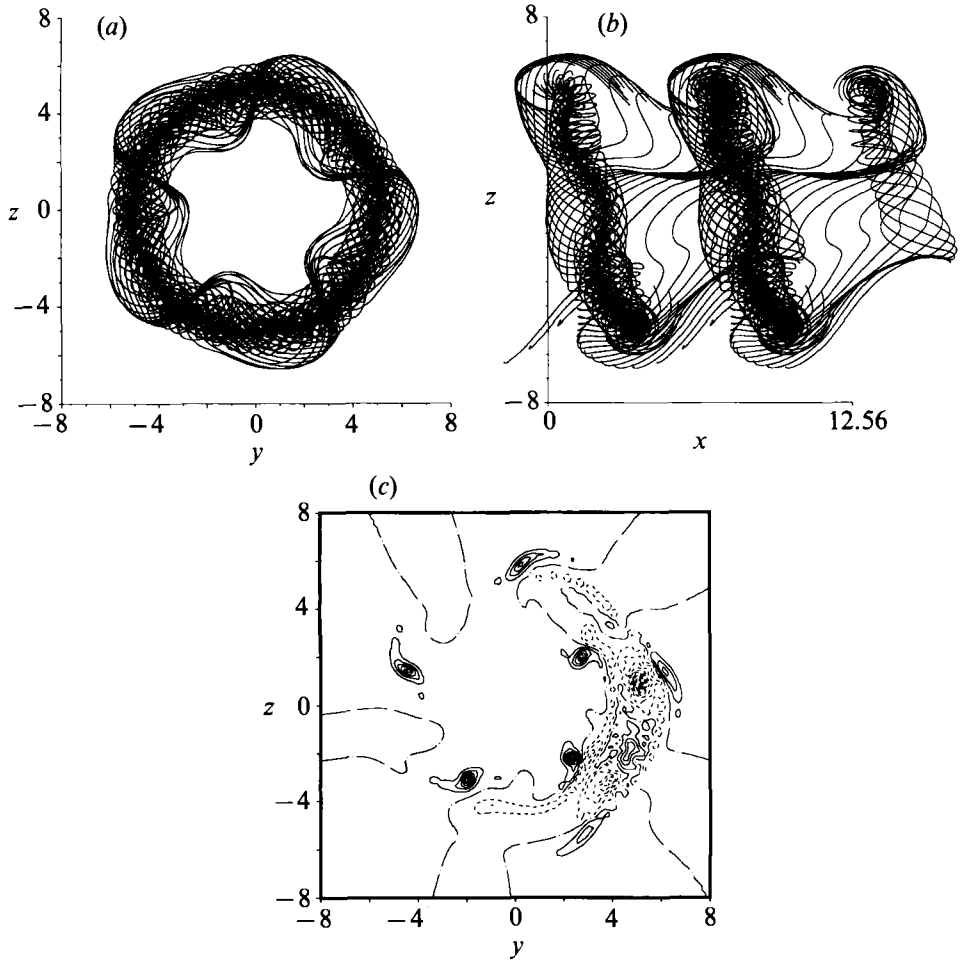

FIGURE 11. The $m = 1$ helically perturbed jet at time 15.70 under the additional influence of a periodic perturbation in the azimuthal direction. (*a*) Streamwise view: the radial amplitude of the helix corrugation tends to zero as it rotates into the streamwise direction. (*b*) Side view of the vortex filaments. (*c*) Contours of the streamwise vorticity at $x = 2$. Notice the azimuthal variation in the extent of the collapse of the axial braid structures. Braid vortices in the downstream region between successive segments of the helix experience greater strain and therefore faster collapse.

centreline and that of an exact helix of identical streamwise wavelength. Also shown is the radial amplitude of the waviness of the helix along with the angle γ, where $\tan(\gamma)$ is given by the ratio of streamwise and radial deviational amplitudes. Variation in γ will then illustrate a rotation of the helix. The initial downswing in the streamwise amplitude suggests that, for early time, when the vortex is weak, global induction dominates the evolution of the helix. Local induction then sends the helix through zero streamwise deviational amplitude. By the final time of the simulation, the streamwise amplitude begins to level off. The radial amplitude of the vortex helix is constant until about time $t = 10$ when it begins to decrease as a result of being rotated in the streamwise direction. In this way, a strong increase in the modulation to the vortex helix, by means similar to the translative instability of the Widnall-type instability, is prevented.

Figure 11 shows the final time of simulation at time $t = 15.70$. The streamwise view of the filaments shows the near elimination of radial corrugation in the vortex helix.

The side view shows the minor increase in the streamwise modulation of the vortex helix as it continues its rotation. The streamwise vorticity contours indicate the increasingly concentrated nature of the single-signed braid vortices. The braid vortices become apparent in the side view of the filaments as well. Portions of the filament centrelines concentrate into a streamwise pattern within the braid region. Once the helical symmetry is broken and concentrated braid vortices can form via the Kelvin–Helmholtz instability, they are candidates for the collapse predicted by Lin & Corcos. For a fixed streamwise location, the braid vortices vary in their concentration and structure based both on their azimuthal location (which determines their proximity to the helix) and whether a braid is inside the helix or is emerging again on the outside of the helix (figure 11*c*). Those braid vortices that are located at a greater distance from the helix are less concentrated. Where a braid passes inside the helical vortex it collapses to nearly circular form, while portions of the same braid that are wrapped to the outside of the helix remain flattened.

Referring to the extensional strain field of the helix-dominated jet given in figure 4(*e*), at a greater distance from the helix, the extensional strain rate is in general smaller than in regions closer to the helix. In particular, regions slightly upstream of the helix experience a more intensive strain than the regions downstream of the helix where braid vorticity is wrapped around the outside. This suggests a dependence of the resulting braid structure on the overall strain field. The same dependence is found in the Lin & Corcos (1984) model of streamwise braid collapse in the plane mixing layer. In their study, collapse of a braid vortex occurs owing to the resultant inward velocity from the (constant) plane strain set up by the spanwise rollers and the self-induced velocity of the streamwise vorticity layer. In this model problem, the imposed extensional strain field acts exclusively in the streamwise direction.

Comparison of the collapse times in the Lin & Corcos study and that occurring in the present investigation is difficult. The variation of the strain rate with time, which occurs in the jet, and the temporal dependence of a braid's circulation strength distinguish the vortices of the jet from the model problem of Lin & Corcos where the circulation of a streamwise vortex changes only as a result of diffusion and a constant rate of plane strain on a vortex is maintained. Furthermore, although their aspect ratios are roughly of the same order before collapse, a comparison of the times involved for the collapse of braid vortices in helix-dominated jets and ring-dominated jets is also complicated by some of the differences between the two cases. On the one hand, for the helix-dominated jet, the diversion of the extensional and compressive strain into the circumferential direction might suggest an increase in time for such a collapse to occur over the time required for the same evolution of braid vortices in a ring-dominated jet. On the other hand, the time for collapse in a given-aspect-ratio vortex depends not only on the strain it experiences, but also on the strength of the braid vortex. Since the braid vorticity is continuously reoriented into the streamwise direction by the primary instability, and since concentrated braid vortices emerge by way of the Kelvin–Helmholtz instability in the helix-dominated jet, the strengths of the braid vortices in the two jets dominated by rings and helices follow different evolutions, making a comparison of their collapse times less meaningful. We plot in figure 12 the circulation versus time of a braid vortex occurring under the present Kelvin–Helmholtz instability (cf. figure 16, Martin & Meiburg 1991*a* for the case of the ring-dominated jet). Although still approximately linear, the growth rate of circulation within a braid vortex is greater than the increase in strength of the counter-rotating braid vortices of the ring-dominated jet.

To quantify the braid instability in the helix-dominated jet, we plot in figure 13

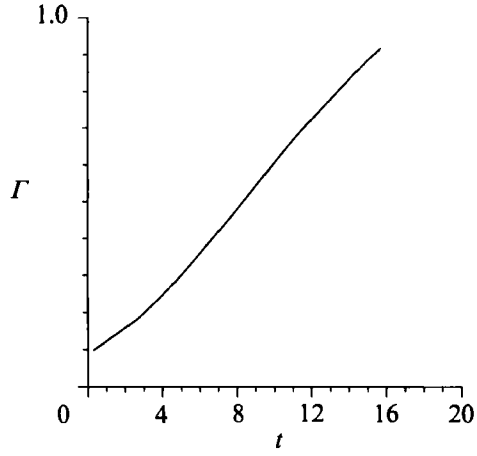

FIGURE 12. The circulation of the streamwise braid vortex as a function of time. Increase in the circulation occurs nearly linearly. The growth rate of the circulation of a braid vortex occurring under the Kelvin–Helmholtz instability in helix-dominated jets is increased over that occurring in the braid vortices of a ring-dominated jet (cf. fig. 16, Martin & Meiburg 1991*a*).

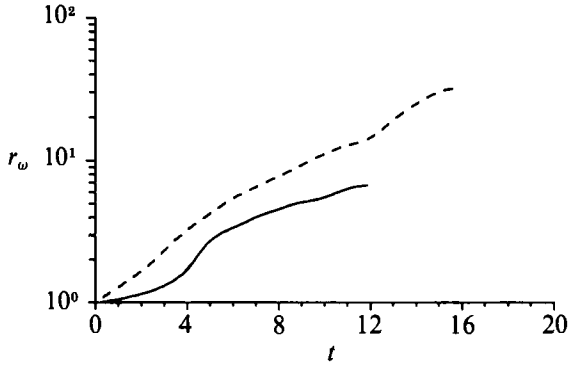

FIGURE 13. Growth of the ratio r_ω of the maximum streamwise braid vorticity to its initial value as a function of time: ——, $m = 1$ helical wave calculation; – – –, $m = 1$ helical wave calculation with additional equal-amplitude radial disturbance resulting in a Kelvin–Helmholtz instability of the braid vorticity layer.

the evolution of the ratio r_ω of maximum streamwise braid vorticity to its initial value. We show the two cases of helical waves with and without additional corrugation. For a helical perturbation only, the growth in the maximum streamwise vorticity is due to the reorientation of the initially circumferential vorticity into the streamwise direction and its subsequent stretching in the time-dependent strain field set up by the evolving helix. Helical symmetry, however, does not allow for the concentration of the streamwise vorticity. This changes when an azimuthal perturbation is introduced as well. Now the Kelvin–Helmholtz instability of the braids produces nearly exponential growth in r_ω. An expression for r_ω for braids undergoing collapse has been given by Lin & Corcos (1984). Again, comparison with their results is not meaningful since the braids of their study do not undergo an evolving strain field and their strength changes only under the action of diffusion.

Figure 14(*a*) illustrates the varying degrees of extensional and compressive strain

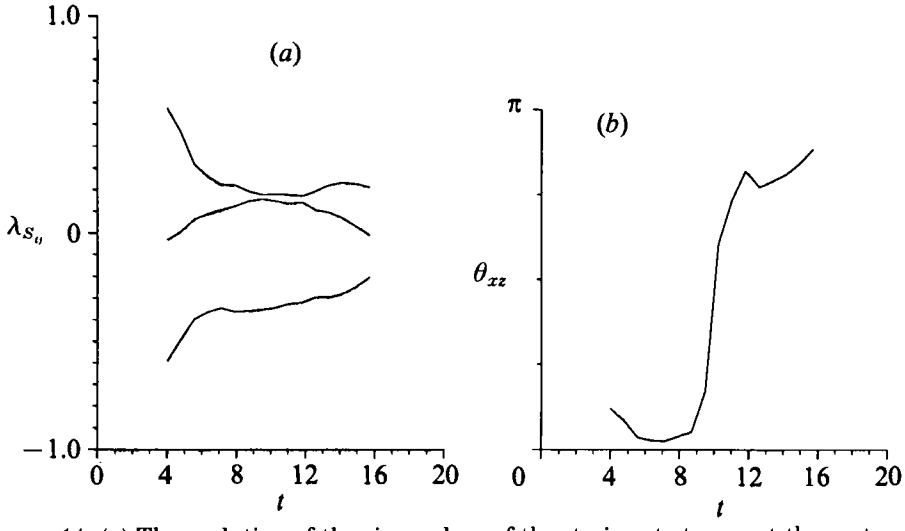

FIGURE 14. (*a*) The evolution of the eigenvalues of the strain rate tensor at the centre of a braid vortex. Eigenvalues are plotted separately based strictly upon their magnitude. Calculations are performed for the braid vortex whose final location at time 15.70 is given by $y = 2.4$, $z = -2.24$ in figure 11 (*c*). (*b*) The direction of the eigenvector in the (x, z)-plane corresponding to the eigenvalue whose magnitude is largest in time. This eigenvector represents the direction of maximum extensional straining placed upon a braid vortex. Although the direction of maximum extensional straining begins by pointing in the direction approximately perpendicular to the vortex helix, it later switches to a direction parallel to the helix.

that a braid vortex is subject to in time. We plot the evolution of the three eigenvalues of the strain tensor as it occurs at the centre of the braid vortex located in the quadrant $y > 0$, $z < 0$ and streamwise location $x = 2$. Referring in particular to the side view of the filaments in figure 11 (*b*), the y- and z-locations of the braid centre and the position where we perform the calculation at the final time of the simulation are given by $y = 2.4$ and $z = -2.24$. We plot the eigenvalues separately based on their magnitude. Figure 14 (*b*) shows the angle in the (x, z)-plane of the eigenvector associated with the eigenvalue whose magnitude remains largest throughout the simulation. The direction of the eigenvector then determines the direction of greatest extensional strain placed upon the braid vortex. The strain rate on a braid is initially high as the vortex helix begins to deplete the braid region of its vorticity. The extensional strain vector within the braid begins by pointing 21.71° in the (x, z)-plane. As expected, extensional strain points in the direction approximately perpendicular to the vortex helix. The line perpendicular to a helix of radius identical to the initial radius of our jet and of streamwise wavelength equivalent to the vortex helix, forms an angle of 17.44°, as sketched in figure 15. The extensional strain rate of the maximum eigenvalue reduces considerably with time as the braids begin to lose their vorticity, while the strain rate of the smaller extensional eigenvalues grows to a value comparable to the maximum eigenvalue. The sudden 90° jump in the direction of maximum extensional strain, roughly at time $t = 10$, suggests that the maximum straining motion on a braid vortex is shifted to the direction perpendicular to that of the original overall extensional straining. Eventually, the strain placed upon a streamwise braid vortex in the direction approximately parallel to the helical vortex reaches levels greater than the extensional straining occurring perpendicular to the helical vortex. This is in

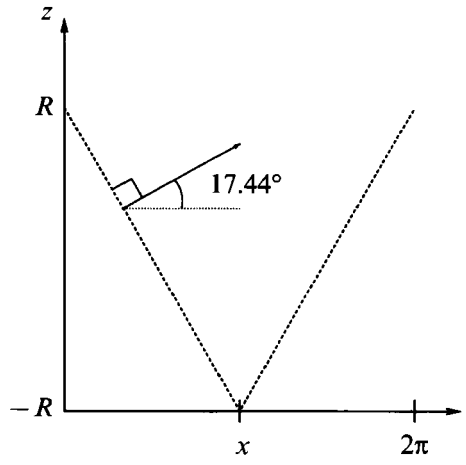

FIGURE 15. Sketch of a helix, drawn in the (x, z)-plane, of wavelength 2π and radius $R = 5$ with its normal direction indicated. The angle of extensional strain in the braid region of the helix-dominated jet begins by pointing in a direction which is approximately perpendicular to the vortex helix of the same wavelength and approximate radius.

contrast to the remarks made by Lin & Corcos for the plane mixing layer. There it was found that the strain in the streamwise direction was always of greater magnitude than any occurring in the plane of the spanwise rollers. The explanation for this switch in the direction of maximum extensional straining in the helix-dominated jet is the strain generated between neighbouring single-signed, streamwise braid vortices.

2.3. *Influence of the azimuthal wave amplitude*

In this section, we analyse the interplay between the helical wave and the azimuthal wave by systematically varying the azimuthal wave amplitude, while leaving the azimuthal wavenumber at the constant value of 5. In all cases, we set the helical displacement amplitude ϵ_1 to 5% of the jet radius, i.e. the displacement of an initially axisymmetric filament centreline by the helical perturbation wave is given as

$$x' = \epsilon_1 R \cos(\alpha x + \phi) = 0.05 R \cos(\alpha x + \phi).$$

The radial displacement is characterized by the azimuthal perturbation amplitude ϵ_2, so that the initial radial position of the filament centreline takes the form

$$r = R(1 + \epsilon_2 \cos(5\phi)).$$

We maintain the ratio R/θ at the value of 22.6 and the streamwise wavenumber α at 1, so that we can compare with the cases $\epsilon_2/\epsilon_1 = 0$ and $\epsilon_2/\epsilon_1 = 1$ considered in §§2.1 and 2.2, respectively. The two additional cases we will consider in this section differ from the flows analysed in §§2.1 and 2.2 in their azimuthal wave amplitudes $\epsilon_2 R$. In particular, we will study the cases of $\epsilon_2/\epsilon_1 = 0.1$ and $\epsilon_2/\epsilon_1 = 0.3$. The dominant helical structure in these flows develops similarly to the previously considered cases in that the streamwise vorticity of the helical vortex is of opposite sign compared to that of the braid. However, the effect of the corrugation becomes increasingly evident for larger values of ϵ_2/ϵ_1, leading to more concentrated braid structures and a dominant vortical structure whose shape deviates more and more from that of a perfect helix.

The streamwise vorticity contours shown in figure 16 for approximately identical

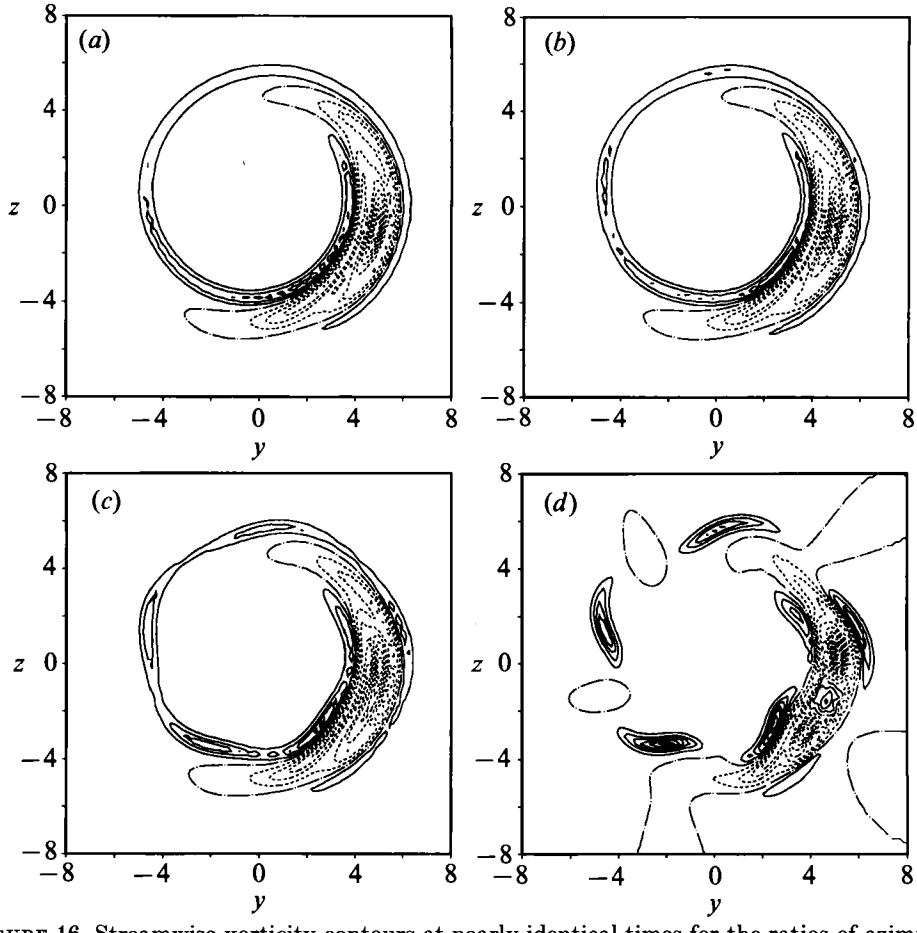

FIGURE 16. Streamwise vorticity contours at nearly identical times for the ratios of azimuthal to helical perturbation amplitude of (*a*) 0, (*b*) 0.1, (*c*) 0.3 and (*d*) 1. While even small azimuthal perturbations lead to a concentration of the braid vorticity, this concentration proceeds faster for larger azimuthal perturbation amplitudes.

times provide a measure of the increasing three-dimensionality of the jets as ϵ_2/ϵ_1 is varied. For all cases shown, the difference between successive contour levels is the same. We recognize that even the smallest azimuthal wave amplitude corresponding to the case $\epsilon_2/\epsilon_1 = 0.1$ leads to a moderate concentration of the braid vorticity. Thus, while a critical azimuthal wave amplitude for braid vorticity concentration to occur does not appear to exist, it is obvious that this concentration happens much more slowly as ϵ_2 is decreased. This can easily be understood in terms of the Lin–Corcos mechanism for the collapse of the braid vorticity. While the external strain on the braid, which is mostly a function of the emerging helical vortex, develops nearly identically for the present set of flows, the second component necessary for the collapse of the streamwise vorticity, i.e. the self-induced velocity of the emerging streamwise structure, is much weaker as ϵ is reduced. This much slower evolution is also reflected in figure 17, which depicts the ratio of the instantaneous maximum streamwise vorticity to its initial value for the various cases. For the case of a helical wave only, r_ω increases only as a result of the reorientation of the filaments in the strain field set up by the emerging helical vortex. However, as soon as there is an

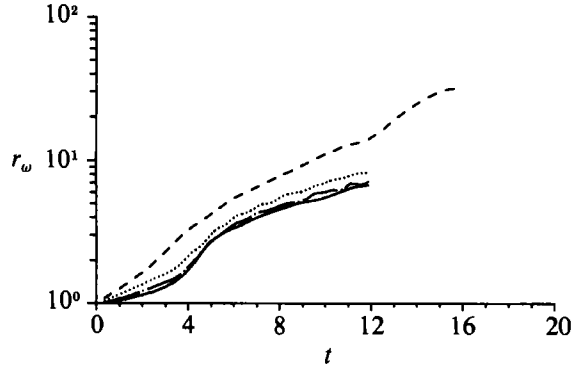

FIGURE 17. Ratio of the maximum streamwise braid vorticity to its initial value for various ratios of azimuthal to helical perturbation wave amplitudes. Higher azimuthal perturbation wave amplitudes lead to a more rapid concentration of the streamwise braid vorticity into large scale braid vortices. Helical 5% and: —, azimuthal 0; —·—, azimuthal 0.5%; ....., azimuthal 1.5%; ----, azimuthal 5%.

additional azimuthal wave, the resulting concentration of the braid vorticity into large-scale streamwise structures leads to an accelerated growth of the maximum streamwise vorticity. The fact that in figure 17 the transition between the purely helical and the $\epsilon_2/\epsilon_1 = 1$ case is smooth underlines again that there is no threshold value for ϵ_2 that has to be exceeded for braid vorticity concentration to occur.

An important question to ask concerns the asymptotic strength of the braid vortices for long times, especially as a function of the azimuthal perturbation amplitude. In our earlier study, we had found that in ring-dominated jets the formation of counter-rotating streamwise braid vortices proceeded more slowly for smaller amplitude azimuthal perturbation waves. Hence, most of the braid vorticity had already become entrained into the large-scale rings before a significant reorientation into the streamwise direction could take place. In this way lower amplitude azimuthal perturbations resulted in weaker braid vortices. For helically dominated jets, the situation is qualitatively different. Independent of the azimuthal wave amplitude, each vortex filament, as it has to remain connected, has to be part of the braid in some region. Hence, as one follows the helical braid once around the jet, the number of filaments that form the braid is not a function of the azimuthal wave amplitude, but only of the streamwise wavenumber of the helical perturbation wave. In this way, the circulation contained in the braid over one helical turn is directly proportional to the streamwise wavelength of the helical perturbation. If we assume that for long times all of the braid circulation becomes concentrated in n streamwise braid vortices, where n is the azimuthal wavenumber, we recognize that the circulation of a streamwise braid vortex should approach a value

$$\Gamma = \frac{\Delta U}{\alpha n}$$

where ΔU is the velocity difference between the jet centreline and the far field. We can summarize then that, in contrast to the ring-dominated jet, where the asymptotic circulation of the streamwise braid structures is a function of the streamwise and the azimuthal wave amplitudes, those parameters should not affect the long-time strength of the braid vortices in helical jets.

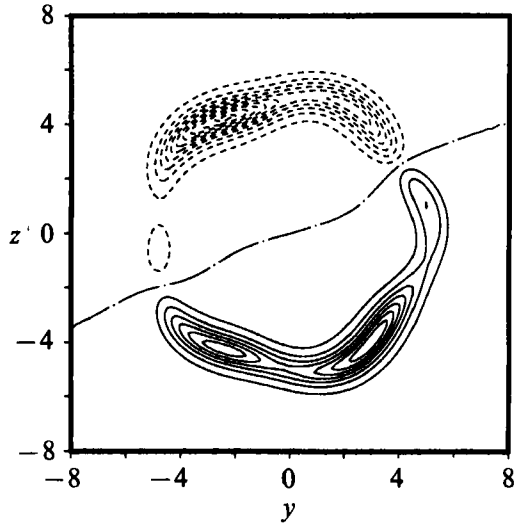

FIGURE 18. Evolution of an axisymmetric jet with $R/\theta = 11.3$ perturbed by a helical wave of azimuthal wavenumber $m = 1$ as well as by an additional azimuthal wave that introduces radial perturbation vorticity corresponding to a corrugated nozzle. Contours of the streamwise vorticity at $x = 9$ for time 0.62 are shown. The initial evolution differs from the corrugated jet with $R/\theta = 22.6$ in a number of respects. Both the positive layer of streamwise braid vorticity and the concentrated region due to the vortex helix are thickened. The braid vorticity layer has multiple maxima of streamwise vorticity indicating an increased initial modulation to the braid vorticity.

2.4. *Influence of the ratio R/θ*

By decreasing a jet's ratio of R/θ to a value of 11.3, we observed in our study of ring-dominated jets a corresponding instability in the primary vortical structure. Decreasing R/θ produced an increase in the core radius of the emerging ring-like vortices. By increasing the core radius while maintaining the strength of a ring, vortex rings become receptive to a longer wavelength for instability (Widnall *et al.* 1974). The increase in core radius of the jet's rings reduced their rotation and instability of the type described by Widnall and associates for isolated vortex rings resulted. We now discuss the influence of a reduction in the ratio R/θ upon the evolution of a jet dominated by a helical vortex. We will address the question of whether similar instabilities occur for the helix of a jet of reduced ratio R/θ. To increase the initial momentum thickness θ of the jet, we double the initial core radius of a filament to 1.0. As in §2.2, we introduce a helical wave along with a radial displacement of equal amplitude in the form of a fivefold-periodic azimuthal wave. The decrease in R/θ makes it necessary to again select the streamwise wavelength for maximum amplification in the linear regime. For $R/\theta = 11.3$ the results of Michalke & Hermann (1982) predict a streamwise wavelength of approximately 3π. In figure 18, we give streamwise vorticity contours at the streamwise location $x = 9$ early in the calculation at time $t = 0.62$. Both the positive layer of braid vorticity and the beginning trace of a vortex helix are markedly thickened. Later in time, the side view at $t = 8.91$ (figure 19) shows a small modulation beginning to form in the emerging helix, while the streamwise vorticity contours demonstrate the dominant occurrence of positive streamwise braid vorticity. The Kelvin–Helmholtz instability again produces strong streamwise vortices within the braid region. There is, however, evidence of weaker opposite-signed streamwise braid vorticity in the braid region.

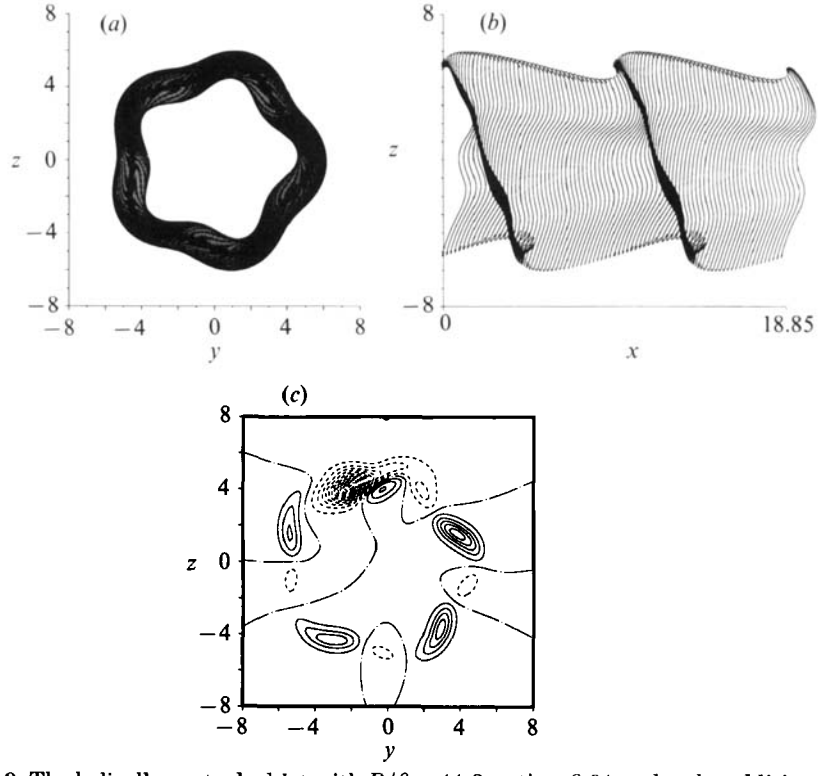

FIGURE 19. The helically perturbed jet with $R/\theta = 11.3$ at time 8.91 under the additional influence of a periodic perturbation in the azimuthal direction. (*a*) Streamwise view. The side view (*b*) shows the emerging helical vortex. The Kelvin–Helmholtz instability of the braid vorticity layer produces strong positive-signed streamwise braids in the streamwise vorticity contour shown in (*c*) for $x = 9$, while the increased effect of global induction leaves remnants of a counterrotating streamwise vortex pair.

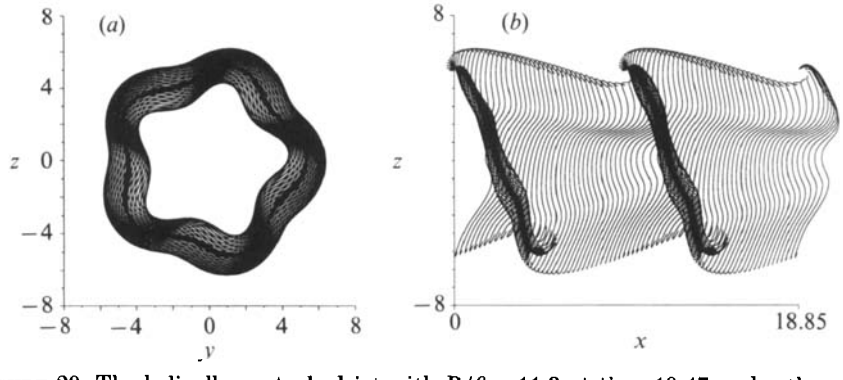

FIGURE 20. The helically perturbed jet with $R/\theta = 11.3$ at time 10.47 under the additional influence of a periodic perturbation in the azimuthal direction: (*a*) streamwise and (*b*) side view.

Global induction has a longer lasting effect on the braid region of decreased ratio R/θ jets, as the outer sections of a filament within the braid region continue to trail ones nearer to the jet axis. The streamwise view of the filaments at times 10.47 and 19.84 (figures 20 and 21) show an increased radial corrugation in the vortex helix. The streamwise vorticity contours illustrate the evolution of the Kelvin–Helmholtz instability within the braids.

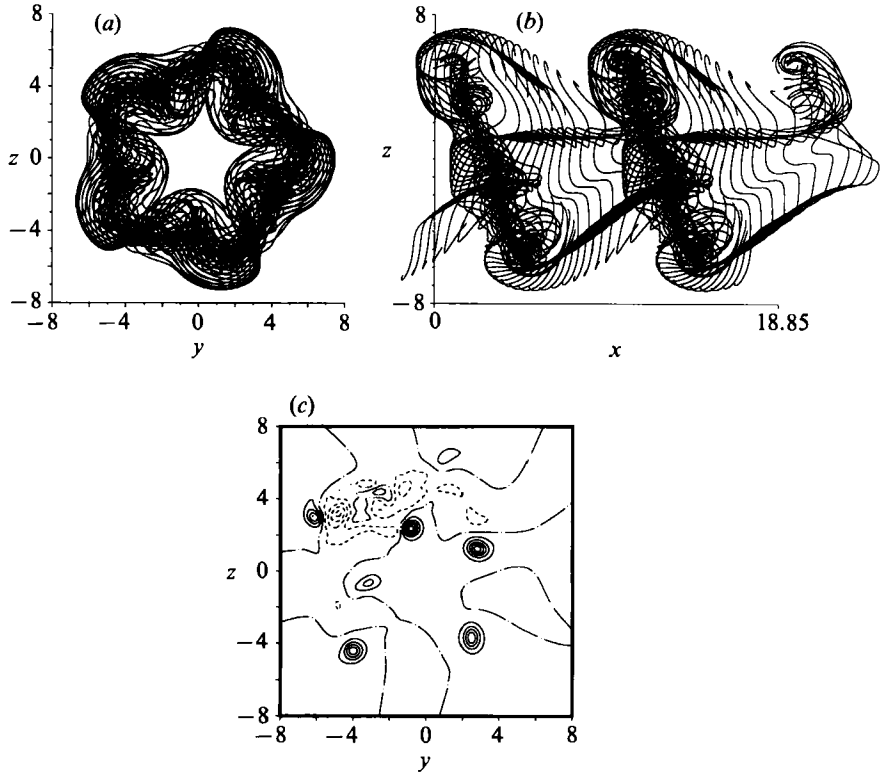

FIGURE 21. The helically perturbed jet with $R/\theta = 11.3$ at time 19.84 under the additional influence of a periodic perturbation in the azimuthal direction: (*a*) Streamwise view: single-signed braid vortices induce an asymmetry in the remaining corrugation of the helix. (*b*) side view and (*c*) contours of the streamwise vorticity at $x = 9$.

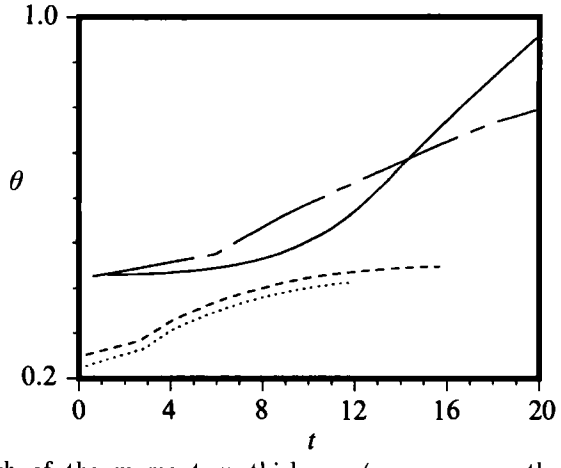

FIGURE 22. Growth of the momentum thickness (average over the circumference and one streamwise wavelength) as a function of time: ....., helical wave calculation, $R/\theta = 22.6$; – – –, helical wave with additional equal-amplitude azimuthal corrugation, $R/\theta = 22.6$; – – –, helical wave with additional equal-amplitude corrugation, $R/\theta = 11.3$; ------, results from the ring-dominated, corrugated jet with $R/\theta = 11.3$ undergoing ring instability.

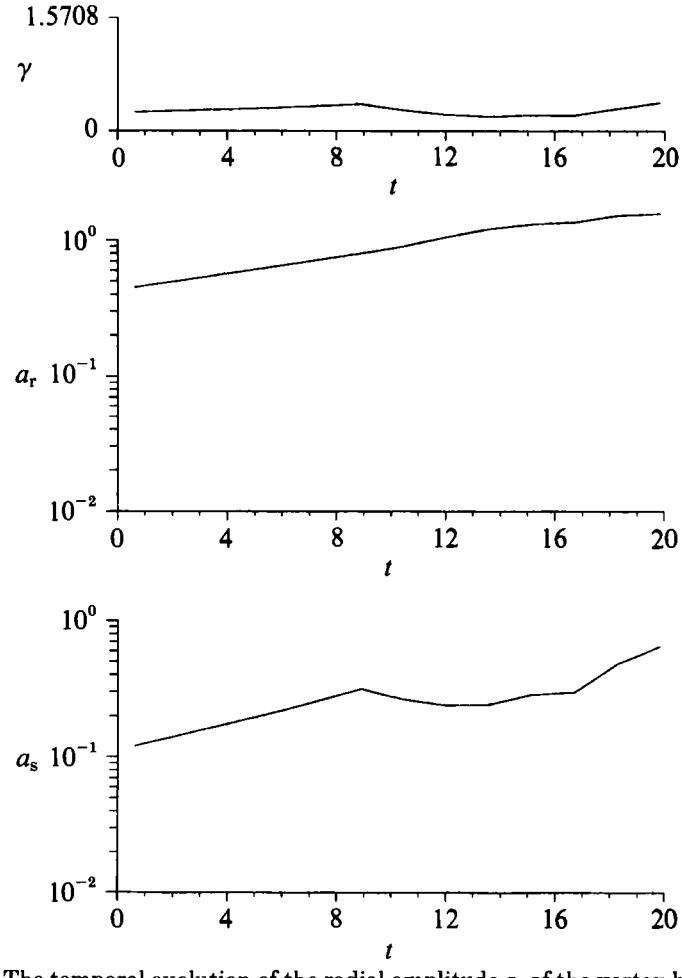

FIGURE 23. The temporal evolution of the radial amplitude a_r of the vortex helix waviness and the streamwise amplitude a_s of the vortex helix's deviation from a perfect helix of equal streamwise wavelength for the jet of ratio $R/\theta = 11.3$. Also plotted is the value γ, where a change in γ indicates rotation of the helix. The rotation of the helix is substantially reduced over earlier considered cases.

In Figure 22 we plot the growth with time of the spatially averaged momentum thickness. Included is the case of the axisymmetric jet undergoing vortex ring instability, along with other cases considered earlier in the present study. While, as pointed out above, the details of the temporal evolution are not necessarily reproduced correctly by the simulation, we can still identify some principal differences between the individual cases. In the strongly helix-dominated flows, the spatial average encompasses a more extensive streamwise region of growth than in ring-dominated jets, where roll-up occurs over only a small portion of the streamwise wavelength. In figure 22, this results in the appearance of initially higher levels of growth in jets experiencing helical roll-up. Most importantly, figure 22 indicates that the evolution of the helix-dominated and ring-dominated jets of equivalent reduced ratio R/θ each follow separate trends. By the final time of the simulation, the momentum thickness of the helix-dominated jet with $R/\theta = 11.3$ tends to level off more strongly than that of the ring-dominated jet of equivalent R/θ. Figure 23 again looks at the temporal evolution of the radial (a_r) and the streamwise(a_s) components

of the vortex helix waviness. The helix almost does not rotate at all, as indicated by the lack of change in γ, while the radial amplitude of the helix waviness grows in near exponential fashion. If we again assume that the mechanisms behind helix instability and ring instability are similar, then the results of figure 23 indicate that the criterion for helix instability are met.

In an effort to compare our numerical results with previous analytical studies performed on isolated helical vortices, we notice that, unfortunately, much less work has been done on the stability of the helical vortex as compared to vortex rings. Motivated by evidence of helical structure in the wake of flat plates and circular cylinders, Levy & Forsdyke (1928) performed an early study on the stability of helical vortices. Widnall (1972) expanded their work by including the added effect of a finite core in the stability analysis. Unfortunately, the analysis is valid only for wavelengths which are long in comparison to the core radius of the helix, although consideration of the short-wavelength instability is given. The helical vortices of Widnall's study provide the most appropriate model known to us for the behaviour of the helical vortex within the jet. In making any comparisons, however, a number of distinctions must be kept in mind. Widnall's analysis is performed on a helical filament of constant vorticity distribution across a circular core. In the jet, the helical vortex emerges with time. Its vorticity distribution displays a corresponding temporal evolution. Furthermore, the analysis of an isolated helical vortex does not include the added influence of braid vorticity which occurs in the jet. In Widnall's study, a small perturbation was taken along the helix. The stability problem then tracks the growth of the perturbation due to the self-induced velocity of the helix. The perturbation was in the radial and/or streamwise directions. Widnall observed three forms of instability of helical vortex filaments: an instability due to mutual induction between turns of the helix, a long-wavelength instability and a short-wavelength instability similar to the short-wavelength instability found for vortex rings. Instability due to mutual induction occurred when streamwise successive turns of the helix passed within a distance one helix radius of one another. A distinctive feature of the helix (as opposed to a ring) is that a non-integer number of disturbance waves per cycle of the helix can be considered. Therefore, streamwise successive segments can be out of phase in their perturbation. Widnall discovered strong evidence of the mutual induction instability only for cases when the perturbation was 180° out of phase on successive segments. Segments of the helix then paired in a manner similar to the helical pairing instability discussed by Pierrehumbert & Widnall (1982) for spatially periodic shear flows. For our case, the azimuthal perturbation imposed upon the jet is uniform along the streamwise wavelength. Successive segments of the vortex helix of the jet, occurring in successive periodic images on the control volume, are then in phase in their perturbation. Therefore we do not expect a similar instance of mutual induction instability in the helical vortex of the jet under the form of azimuthal perturbation considered.

Widnall documented the long-wavelength instability for values of the number of waves per cycle of less than KR, where K is the streamwise wavenumber of the helix and R its radius. For our case, the vortex helix has the same streamwise wavenumber as the wavelength of the jet within which it occurs. Therefore for the case of $R/\theta = 11.3$, K is equal to $\frac{2}{3}$. The corrugation imposes a value of 5 waves per cycle onto the vortex helix, a value which places the helix of this jet outside the valid region for long-wavelength instability to occur. Widnall furthermore explained how the short-wavelength instability could be similar to the short-wavelength instability in vortex

rings. It was expected that for very short wavelengths, only the influence of neighbouring portions of the helix would have large effect. The short-wave instability, being a local property of a vortex filament, would then behave similarly in both rings and helices. A latter study done on short-wave instability in vortex rings (Widnall *et al.* 1974) suggested, however, that short-wave instability in the vortex ring might be in part caused by the strain induced by the remaining portions of the ring. Clearly the strain field of a vortex helix differs from that of a vortex ring. Therefore it is not entirely clear how well-suited the results from the instability of vortex rings are to the vortex helix. Unfortunately, the short-wavelength instability falls outside the region of validity of Widnall's helical vortex analysis.

A similar difficulty occurred in the long-wavelength stability analysis of vortex rings (Widnall & Sullivan 1973). The wavelength for instability discovered lay outside the wavelengths for which the analysis was considered valid. The analysis was then extended (Widnall *et al* 1974). To our knowledge, a similar study, valid for short-wavelength disturbances on helical vortex, has not yet been performed. Therefore a thorough quantitative comparison with the necessary parameters for a short-wavelength instability is impossible. In the study of helical vortices, Widnall did, however, present the characteristic lengthscale of the short-wavelength vortex helix instability. The study also demonstrated how it might be applied to the results on vortex rings. Following Widnall (1972), the characteristics lengthscale for the short-wavelength instability in the helix is its local radius of curvature

$$S = \frac{1 + K^2 R^2}{R K^2}.$$

Then, a measure of helical vortex core size, for use in the results on vortex rings, becomes aS/R, where a is the core radius of the helical vortex. For the present streamwise wavelength and radius, the core radius used for the evaluation of the effective wavenumber for instability in the vortex helix is increased by 9% over the value used for vortex rings of identical core radius. Keeping in mind that the helical vortex is continually evolving in the jet, one should again anticipate instability in the helical vortex of the $R/\theta = 11.3$ jet at some point in the flow evolution, as was found in the rings of the equivalent-parameter ring-dominated jet, since the increase in measure of core radius in helices is only very slight, and roll-up evolves in a similar fashion. However, we expect that as the helical vortex emerges, the necessary parameters for its instability occur at a slightly different time than they do for the ring-like vortices of similar ring-dominated jets.

3. Summary and conclusions

Our aim has been a more complete understanding of some of the inviscid mechanisms in the three-dimensional evolution of an axisymmetric jet. In earlier studies we considered jets whose primary vortical structure was excited by axisymmetric perturbation. Within the present study, we have extended this analysis by considering the nonlinear, three-dimensional evolution of jets whose primary structure are helical in nature. The results of a helically symmetric calculation form the basis for our subsequent discussion of helix-dominated jets. By including a single helical mode of azimuthal wavenumber 1, the individuality of ring-like vortices under axisymmetric perturbation is replaced by a single vortex of helical form, connected by a braid region. Helical symmetry mandates the formation of a single-signed sheet-like braid vorticity layer. While the vortex rings that occur under

axisymmetric disturbance limit the spanwise extent of the braid vorticity of one sign, the aspect ratio of the layer of braid vorticity of one sign in a helix-dominated jet tends to an infinite value.

Primary structure in the form of a helical vortex creates an additional circumferential component in the overall strain field. In the jet, the strain field exhibits an upstream–downstream asymmetry about the primary vortical structure, whether the structure is helical in nature or in the form of a vortex ring. Based on the findings of Lin & Corcos for infinite-aspect-ratio braid vorticity regions in the mixing layer, the formation of single-signed structures appears likely. By introducing an additional perturbation in the azimuthal direction, thereby breaking the helical symmetry, a Kelvin–Helmholtz-like instability evolves within the braid region. In this way, streamwise braid vortices evolve, which are indeed all of the same sign of vorticity. This development of single-signed streamwise braid vortices is in contrast to the counter-rotating structures which form in the braid regions of the jet under axisymmetric disturbance. Further concentration of the single-signed braid vortices occurs due to the extensional strain field set up by the strengthening helix, in the same manner as the collapse of the finite-aspect-ratio counter-rotating vortices seen in the ring-dominated jet of Martin & Meiburg (1991*a*) and described by Lin & Corcos. With the additional azimuthal perturbation to the jet, the helix develops wavy modulations. The continuing rotation of the helix, in the jet of ratio $R/\theta = 22.6$, does not allow instability in a manner which is similar to the translative instability described by Pierrehumbert & Widnall (1982) for periodic shear layers, as it prevents the amplitude of the waviness in the helix from growing in the overall strain field. By varying the ratio between the amplitude of the helical and radial disturbances, the initial form the braid vorticity can be strongly influenced. However, we find that the long-time strength of the concentrated braid vortices should not depend on the streamwise and azimuthal perturbation amplitudes, but rather on the wavenumbers.

For a jet of $R/\theta = 11.3$, we observe the initial, near-exponential growth of the amplitude of the helix waviness. As we have seen for ring-dominated jets of decreased R/θ, the increase of the momentum thickness increases the initial core radius and alters a vortex's self-induced velocity. In a jet with $R/\theta = 11.3$ under axisymmetric and additional azimuthal perturbation, we observed a corresponding reduced rotation rate and the occurrence of a Widnall-type instability of the rings creating large amplitudes in their waviness by the end of simulation. For the helix-dominated jet with $R/\theta = 11.3$, and with the same additional fivefold corrugation, we again initially observe the reduction in rotation of the helical vortex and the near exponential growth of its waviness, characteristic of vortex helix instability.

Future topics of interest include the question of how the helical structures grow in the streamwise direction. On this issue, some guidance is provided by the experimental study of Browand & Laufer (1975). Further interesting problems are posed by the interaction of helical perturbations of different wavenumbers, as well as by the evolution of jets simultaneously perturbed by helical and axisymmetric waves. A very interesting additional topic concerns the simulation of jets with swirl.

This work has been supported by the National Science Foundation under grant CTS-9058065 and by the Electric Power Research Institute under project RP8006 to EM, and by DARPA under URI contract N00014-86-K0754 to Brown University. The San Diego Supercomputer Center has been providing computing time on its CRAY-Y/MP.

REFERENCES

ACHENBACH, E. 1974 Vortex shedding from spheres. *J. Fluid Mech.* **62**, 209.

ASHURST, W. T. & MEIBURG, E. 1988 Three-dimensional shear layers via vortex dynamics. *J. Fluid Mech.* **189**, 87.

BATCHELOR, G. K. & GILL, A. E. 1962 Analysis of the stability of axisymmetric jets. *J. Fluid Mech.* **14**, 529.

BROWAND, F. K. & LAUFER, J. 1975 The role of large scale structures in the initial development of circular jets. In *Proc. 4th Biennial Symp. Turbulence in Liquids, Univ. Missouri-Rolla*, pp. 333–344. Princeton, New Jersey: Science Press.

CHAN, Y. Y. 1976 Spatial waves of higher modes in an axisymmetric turbulent jet. *Phys. Fluids* **19**, 2042.

COHEN, J. & WYGNANSKI, I. 1987*a* The evolution of instabilities in the axisymmetric jet. Part 1. The linear growth of disturbances near the nozzle. *J. Fluid Mech.* **176**, 191.

COHEN, J. & WYGNANSKI, I. 1987*b* The evolution of instabilities in the axisymmetric jet. Part 2. The flow resulting from the interaction between two waves. *J. Fluid Mech.* **176**, 221.

CORKE, T. C. & KUSEK, S. M. 1991 Resonance in axisymmetric jets with controlled helical mode input. *AIAA Paper* 91-0319.

DIMOTAKIS, P. E., MIAKE-LYE, R. C., & PAPANTONIOU, D. A. 1983 Structure and dynamics of round turbulent jets. *Phys. Fluids* **26**, 3185.

GASTER, M. 1962 A note on the relation between temporally-increasing and spatially-increasing disturbances in hydrodynamic stability. *J. Fluid Mech.* **14**, 222.

ILEGBUSI, J. O. & SPALDING, D. B. 1984 A steady-unsteady visualization technique for wake-flow studies. *J. Fluid Mech.* **139**, 435.

KO, N. W. M. & LAM, K. M. 1984 Further measurements in the initial region of an annular jet. *J. Sound Vib.* **92**, 333.

KOCH, C. R., MUNGAL, M. G., REYNOLDS, W. C. & POWELL, J. D. 1989 Gallery of fluid motion. *Phys. Fluids* A **1**, 1443.

KUSEK, S. M., CORKE, T. C. & REISENTHEL, P. 1989 Control of two and three dimensional modes in the initial region of an axisymmetric jet. *AIAA Paper* 89-0968.

LASHERAS, J. C. & MEIBURG, E. 1990 Three-dimensional vorticity modes in the wake of a flat plate. *Phys. Fluids* A **2**, 371.

LEONARD, A. 1985 Computing three-dimensional flows with vortex elements. *Ann. Rev. Fluid Mech.* **17**, 523.

LEVY, H. & FORSDYKE, A. G. 1928 The steady motion and stability of a helical vortex. *Proc. R. Soc. Lond.* A **120**, 670.

LIN, S. J. & CORCOS, G. M. 1984 The mixing layer: deterministic models of a turbulent flow. Part 3. The effect of plane strain on the dynamics of streamwise vortices. *J. Fluid Mech.* **141**, 139.

LOPEZ, J. L. & KURZWEG, U. H. 1977 Amplification of helical disturbances in a round jet. *Phys. Fluids* **20**, 860.

MARTIN, J. E. & MEIBURG, E. 1991*a* Numerical investigation of three-dimensionally evolving jets subject to axisymmetric and azimuthal perturbation. *J. Fluid Mech.* **230**, 271.

MARTIN, J. E. & MEIBURG, E. 1991*b* The three-dimensional evolution of axisymmetric jets perturbed by helical waves. In *Proc. Eighth Symp. on Turbulent Shear Flows, Munich.*

MATTINGLY, G. E. & CHANG, C. C. 1974 Unstable waves on an axisymmetric jet column. *J. Fluid Mech.* **65**, 541.

MEIBURG, E. 1989 Incorporation and test of diffusion and strain effects in the two-dimensional vortex blob technique. *J. Comput. Phys.* **82**, 85.

MEIBURG, E. & LASHERAS, J. C. 1988 Experimental and numerical investigation of the three-dimensional transition in plane wakes. *J. Fluid Mech.* **190**, 1.

MEIBURG, E. & MARTIN, J. E. 1991 The evolution of helical waves on axisymmetric jets. In *Advances in Turbulence 3*, p. 85. Springer. (ed. A. V. Johansson & P. H. Alfredson)

MICHALKE, A. 1971 Instabilität eines kompressiblen runden Freistrahls unter Berücksichtigung des Einflusses der Strahlgrenzschichtdicke. *Z. Flugwiss.* **19**, 319.

MICHALKE, A. & HERMANN, G. 1982 On the inviscid instability of a circular jet with external flow. *J. Fluid Mech.* **114**, 343.

MODI, V. J. & AKATSU, T. 1984 Wall confinement effects for spheres in the Reynolds number range of 30–2000. *Trans. ASME* I: *J. Fluids Engng.* **106**, 66.

MONKEWITZ, P. A. 1988 A note on vortex shedding from axisymmetric bluff bodies. *J. Fluid Mech.* **192**, 561.

MOORE, C. J. 1977 The role of shear-layer instability waves in jet exhaust noise. *J. Fluid Mech.* **80**, 321.

NEU, J. C. 1984 The dynamics of stretched vortices. *J. Fluid Mech.* **89**, 469.

PAO, H. P. & KAO, T. W. 1977 Vortex structure in the wake of a sphere. *Phys. Fluids* **20**, 187.

PIERREHUMBERT, R. T. & WIDNALL, S. E. 1982 The two- and three-dimensional instabilities of a spatially periodic shear layer. *J. Fluid Mech.* **114**, 59.

PLASCHKO, P. 1979 Helical instabilities of slowly divergent jets. *J. Fluid Mech.* **92**, 209.

STRANGE, P. J. R. & CRIGHTON, D. G. 1983 Spinning modes on axisymmetric jets. Part 1. *J. Fluid Mech.* **134**, 231.

TANEDA, S. 1956 Experimental investigation of the wake behind a sphere at low Reynolds numbers. *J. Phys. Soc. Japan* **11**, 1104.

TSO, J. & HUSSAIN, F. 1989 Organized motions in a fully developed turbulent axisymmetric jet. *J. Fluid Mech.* **203**, 425.

WIDNALL, S. E. 1972 The stability of a helical vortex filament. *J. Fluid Mech.* **54**, 641.

WIDNALL, S. E., BLISS, D. B. & TSAI, C.-Y. 1974 The instability of short waves on a vortex ring. *J. Fluid Mech.* **66**, 35.

WIDNALL, S. E. & SULLIVAN, J. P. 1973 On the stability of vortex rings. *Proc. R. Soc. Lond.* A. **332**, 335.